Regulation of CTP Synthase Filament Formation During DNA Endoreplication in *Drosophila*

Pei-Yu Wang,*,† Wei-Cheng Lin,† Yi-Cheng Tsai,‡ Mei-Ling Cheng,§, Yu-Hung Lin,‡ Shu-Heng Tseng,‡ Archan Chakraborty,‡ and Li-Mei Pai*,†,‡,††,1**

*Department of Biochemistry,†Molecular Medicine Research Center,‡Graduate Institute of Biomedical Sciences, College of Medicine,§Department of Biomedical Sciences, **Healthy Aging Research Center, Chang Gung University, and, ††Chang Gung Memorial Hospital, Kwei-Shan, Tao-Yuan, 333 Taiwan

ORCID ID: 0000-0002-1417-6432 (L.-M.P.)

ABSTRACT CTP synthase (CTPsyn) plays an essential role in DNA, RNA, and lipid synthesis. Recent studies in bacteria, yeast, and *Drosophila* all reveal a polymeric CTPsyn structure, which dynamically regulates its enzymatic activity. However, the molecular mechanism underlying the formation of CTPsyn polymers is not completely understood. In this study, we found that reversible ubiquitination regulates the dynamic assembly of the filamentous structures of *Drosophila* CTPsyn. We further determined that the proto-oncogene Cbl, an E3 ubiquitin ligase, controls CTPsyn filament formation in endocycles. While the E3 ligase activity of Cbl is required for CTPsyn filament formation, Cbl does not affect the protein levels of CTPsyn. It remains unclear whether the regulation of CTPsyn filaments by Cbl is through direct ubiquitination of CTPsyn. In the absence of Cbl or with knockdown of CTPsyn, the progression of the endocycle-associated S phase was impaired. Furthermore, overexpression of wild-type, but not enzymatically inactive CTPsyn, rescued the endocycle defect in *Cbl* mutant cells. Together, these results suggest that Cbl influences the nucleotide pool balance and controls CTPsyn filament formation in endocycles. This study links Cbl-mediated ubiquitination to the polymerization of a metabolic enzyme and reveals a role for Cbl in endocycles during *Drosophila* development.

KEYWORDS Cbl; CTP synthase; cytoophidia; endocycle; *Drosophila*

PROVIDING the raw material for DNA/RNA replication is a key challenge faced by all organisms during rapid growth. One particularly interesting example of this challenge is polyploidy, which arises from endoreplication and is essential for the normal development and specific physiological conditions of many diploid organisms. Organisms often use endoreplication, a type of cell cycle encompassing genomic replication without cell division, to provide nutrients to support the developing egg/embryo and enlarged cell size. Examples of cells and tissues that endocycle include mammalian trophoblast giant cells, plant seeds/roots, and *Drosophila* egg chambers (Edgar and Orr-Weaver 2001; Lee *et al.* 2009). In *Drosophila*, embryogenesis requires the mass production of proteins and high metabolic activity, which are achieved through endoreplication in the terminally differentiated cells of the developing egg chamber.

Drosophila oogenesis provides an excellent system for analyzing developmentally controlled endoreplication. Egg production takes place within 16-cell germline cysts, with the asymmetric and incomplete division of a germline stem cell (Calvi and Spradling 1999). After cyst formation, nurse cells immediately exit the mitotic cycle and begin a series of 10–12 endocycles to reach 512C DNA content to provide proteins and messenger RNAs (mRNAs) for the developing oocyte. Each germline cyst is enveloped by 15–20 somatic follicle cells that divide mitotically to form an epithelial monolayer of ~1000 cells and then employ three endocycles to reach 16C DNA content during stages 7–10A, the so-called "endocycle stages" (Klusza and Deng 2011). Endoreplication in the follicular epithelium ensures a large amount of eggshell protein production in <24 h (Lilly and Spradling 1996; Calvi *et al.* 1998). The endocycle in the follicle cells ceases at stage 10B, but some specific genomic foci (*e.g.*, chorion genes) continue to amplify

doi: 10.1534/genetics.115.180737
Manuscript received July 15, 2015; accepted for publication October 13, 2015; published Early Online October 19, 2015.
Supporting information is available online at www.genetics.org/lookup/suppl/doi:10.1534/genetics.115.180737/-/DC1.
[1]Corresponding author: Chang Gung University, 259 Wen-Hwa 1st Rd., Kwei-Shan, Tao-Yuan, 333 Taiwan. E-mail:pai@mail.cgu.edu.tw

synchronously, an event called gene amplification (Calvi *et al.* 1998). Notch signaling is responsible for the mitotic cycle–endocycle transition of follicle cells (Deng *et al.* 2001; Lopez-Schier and St. Johnston 2001), which activates the Cyclin E/Cyclin-Dependent Kinase 2 (CycE/Cdk2) complex to trigger the endocycle transition (Shcherbata *et al.* 2004).

This rapid series of endoreplication events requires cells to have sufficient stores of the raw materials for DNA synthesis. CTP synthase (CTPsyn) produces CTP to facilitate DNA and RNA synthesis. In both prokaryotes and eukaryotes, CTPsyn is allosterically bound to GTP, activating glutamine hydrolysis to generate ammonia (Long and Pardee 1967; Long *et al.* 1970; Levitzki and Koshland 1972). Subsequently, CTPsyn catalyzes the ATP-dependent transfer of ammonia from glutamine to the C-4 position of UTP to form CTP (Lieberman 1956; Chakraborty and Hurlbert 1961; Levitzki and Koshland 1971; von der Saal *et al.* 1985; Endrizzi *et al.* 2004). Under low concentrations of CTPsyn or in the absence of ATP/UTP/CTP, CTPsyn is present as an inactive monomer. With an increasing concentration of CTPsyn, CTPsyn initially forms inactive dimers and then forms active tetramers in the presence of ATP/UTP/CTP (Anderson 1983; von der Saal *et al.* 1985). Therefore, CTPsyn monitors cellular nucleotide pools through its four NTP-binding sites, allowing it to match its activity to the concentration of nucleotides (Aronow and Ullman 1987).

Recently, filamentous CTPsyn structures were independently revealed in bacteria, budding yeast, *Drosophila*, and mammalian cell lines, representing a novel, evolutionarily conserved cellular structure (Ingerson-Mahar *et al.* 2010; Liu 2010; Noree *et al.* 2010; Carcamo *et al.* 2011). In *Caulobacter crescentus*, the CTPsyn filaments (CtpS filaments) interact with intermediate filaments to regulate bacterial shape (Ingerson-Mahar *et al.* 2010). In budding yeast, CTP synthase filaments are promoted under the condition of carbon source depletion (Noree *et al.* 2010). In *Drosophila*, this structure, termed the "cytoophidia," is present in a number of tissues, including the salivary gland, testis, mid-gut, and ovary (Buszczak *et al.* 2007; Liu 2010). Both in yeast and *Drosophila*, the formation of a filament composed of CTPsyn does not require active tetramers, arguing that the filament is composed of inactive CTPsyn dimers or monomers (Aughey *et al.* 2014; Noree *et al.* 2014). However, CTPsyn filaments in bacteria are composed of an inactive form of tetramers (Barry *et al.* 2014). In mammals, this structure, termed "rods and rings" (RR), appears in both the cytoplasm and the nucleus (Gou *et al.* 2014) and acts in a cell cycle-independent manner (Carcamo *et al.* 2011). The RR structure contains not only CTPsyn, but also inosine monophosphase dehydrogenase 2 (IMPDH2), a key enzyme in GTP biosynthesis (Carcamo *et al.* 2011). Recently, the RR structure was recognized as reflecting the concentration of glutamine, an essential amide nitrogen donor in the nucleotide biosynthesis pathway. The depletion of glutamine forced the formation of the RR structure in mammalian cells (Calise *et al.* 2014; Gou *et al.* 2014).

Despite this strikingly broad evolutionary conservation, the function of these filamentous structures and the regulation of their assembly remain elusive. During *Drosophila* oogenesis, germline cells of the ovary contain two different sizes of CTPsyn filaments in one cell; they can be classified into micro-cytoophidia (1–6 μm) and macro-cytoophidia (10–50 μm) (Liu 2010). While we know that increasing the level of CTPsyn in *Drosophila* enhances the formation of cytoophidia structures and that CTPsyn activity seems to correlate with the structure in yeast, bacteria, and *Drosophila* (Chen *et al.* 2011; Azzam and Liu 2013; Aughey *et al.* 2014; Barry *et al.* 2014; Noree *et al.* 2014; Strochlic *et al.* 2014), other mechanisms regulating their assembly remain unknown.

We previously analyzed the function of the proto-oncogene Casitas B-lineage lymphoma (Cbl), which is conserved in *Caenorhabditis elegans*, *Drosophila*, and mammalian cells. It encodes an E3 ligase that plays a negative role in the receptor tyrosine kinase pathway through its ubiquitin ligase activity (Marmor and Yarden 2004). Ubiquitination of the epidermal growth factor receptor (EGFR) promotes endosomal sorting and lysosomal degradation of this protein (Chang *et al.* 2008; Wang and Pai 2011). In this role, Cbl determines the polarity of the developing egg by negatively regulating the EGFR in follicle cells (Pai *et al.* 2000). Cbl can also regulate Notch signaling, an activity related to its short isoform, Cbl-S, during eye and wing development (Wang *et al.* 2010). Cbl has also been implicated in regulating cell proliferation in the germline, although the mechanism is not known (Epstein *et al.* 2009). Here, we describe a novel role for Cbl in promoting the endocycle through regulating CTPsyn activity. Moreover, we reveal that reversible modification of ubiquitin regulates the dynamic assembly of CTPsyn structures, the cytoophidia. Together, our data demonstrate a potential role for cytoophidia during *Drosophila* development and begin to uncover the mechanisms regulating CTPsyn filament assembly.

Materials and Methods

Fly stocks and genetics

The strains used included the following: wild-type (Oregon-R); $Cbl^{F165}/TM3Ser$ (Pai *et al.* 2000); $Cbl^{BB28}/TM3Ser$ (Pai *et al.* 2006); *UAS-λ-top* (Queenan *et al.* 1997); $Pros\beta6^{1}/TM3Sb$ (Saville and Belote 1993); $Hs83\text{-}D\text{-}Cbl\text{-}L\text{-}PR^{Drk}\text{-}75$ (Wang and Pai 2011); *Hs83-D-CblS-2* (Pai *et al.* 2006); *UAS-HA-ubiquitin* (a gift from C. T. Chien, Institute of Molecular Biology, Academia Sinica, Taiwan); *UAS-Dicer2* (Bloomington Stock Center); $UAS\text{-}CTP\ synthase^{GD12759}$ (Vienna *Drosophila* RNAi Center); and *GR1*, *CY2*, and *55B-Gal4* (Queenan *et al.* 1997). For the genetic interaction assay, *OreR*, $Pros\beta6^{1}/+$, and $Cbl^{F165}/Pros\beta6^{1}$ were incubated for 3 days at 18° and then at 29° for 2 days. $e22cFLP/+$; $Cbl^{F165}FRT^{80B}$ (or $Cbl^{BB28}FRT^{80B}$) $/hs\text{-}mycFRT^{80B}$ and $hs\text{-}FLP^{l22}/X$; $Cbl^{F165}FRT2A/ovoDFRT2A$ were used for generating mosaic clones as described previously (Pai *et al.* 2000). $hs\text{-}FLP^{l22}/X$; $Cbl^{F165}FRT^{80B}/[ubi\text{-}nlsRFP]FRT^{80B}$ was used to generate mosaic clones in the salivary glands. Eggs, 2.5–3.5 hr old, were collected, heat-shocked at 37° for 1.5 hr, and developed to 96-hr third instar larvae.

Antibodies

The primary antibodies used for immunohistochemistry included rabbit anti-CTPsyn (1:300; y-88, sc-134457; Santa Cruz), rat anti-HA (1:500; Roche 3F10), mouse anti-MPM2 (1:200; Millipore), mouse anti-Cut (1:50; 2B10); mouse anti-Hnt (1:15 1G9); mouse anti-Flag (1:500; Sigma F1804), and rabbit anti-Myc (1:200; Santa Cruz), while the secondary antibodies included Alexa Fluor 488 or 546 anti-mouse/rabbit/rat antibodies (Molecular Probes). To visualize DNA, 0.5 mg/mL DAPI (Sigma) was added for 5 min at room temperature. To visualize actin, phalloidin (1:100; Molecular Probes) was used. The antibodies used for immunoblotting were anti-D-Cbl 10F1 ascites (Pai *et al.* 2006), rabbit anti-dCTPsyn, and mouse anti-tubulin (Sigma).

Drug treatment

For MG132 treatment, ovaries were dissected in Schneider's insect medium (Gibco) and then were incubated in medium containing 60 μM MG132 (20 mM stock dissolved in DMSO) or DMSO (as a control) for 2 hr at room temperature. For Pr619 plus MG132 treatment, ovaries were dissected in Schneider's medium and then incubated in medium containing 50 μM Pr619 (20 mM stock was dissolved in DMSO) or DMSO for 2 hr at room temperature. After this, the ovaries were transferred to medium containing 60 μM MG132 or DMSO and incubated for another 2 hr at room temperature. After drug treatment, the ovaries were fixed with 4% paraformaldehyde and analyzed by immunostaining.

CTPsyn inhibitor treatment

DON (6-diazo-5-oxo-L-norleucine) (D2141, Sigma) was solubilized at 500 μg/ml in water. Adult females were yeasted for 3–5 days and then fed on wet yeast with or without 500 μg/ml of DON for 24 hr, as previously described (Chen *et al.* 2011).

Bromodeoxyuridine incorporation assays

Ovaries and salivary glands were collected in Schneider's medium and then incubated in a medium containing 30 μg/ml bromodeoxyuridine (BrdU) (Sigma) at room temperature for 1 h. The BrdU-incorporated tissues were fixed in 200 μl of 4% formaldehyde containing 600 μl heptane and 0.25% NP-40 for 20 min at room temperature. The samples were treated with 2 N HCl for 30 min, neutralized with 100 mM sodium borate, and washed with PBT three times. For BrdU detection, the samples were incubated with PBT containing 10% horse serum and then with anti-BrdU antibody (1:50, Becton Dickinson) at 4° overnight. Alexa Fluor 488 goat anti-mouse (1:1000; Molecular Probes) was used as the secondary antibody.

Quantification of BrdU-positive cells

For quantification of the percentage of BrdU-positive cells in the *Cbl* clone, the number of BrdU-positive cells was divided by the total cell number in the *Cbl* clone or its twin clone. To calculate the percentage of BrdU-positive cells for the genetic interaction experiment, we counted BrdU-positive cells in the first five rows of the anterior and posterior follicle cells per egg chamber in *55B-Gal4::UAS-CTPsyn^{RNAi}*, *55B-Gal4::UAS-GFP*, *OreR,CY2-Gal4* in *Cbl* heterozygous mutants and *CY2-Gal4::UAS-CTPsyn$^{RNA\ i}$* with or without *Cbl* heterozygous mutants and then divided this number by the total number of cells in the five rows.

Transgenic line generation and induction

To generate Flag-CTPsyn, a complementary DNA (cDNA) fragment of CTPsyn isoform C was amplified by PCR from an ovarian cDNA library with the specific primers CTPsyn-C-F 5′-GTCTCGAGATGAAATACATCCTGGTAAC-3′and CTPsyn-C-R 5′-GTCTCGAGTTACTTATGGCCATTGGTAG-3′. The CTPsyn fragment was cloned into pUAST-Flag using *Xho*I and *Xba*I restriction enzymes and was in-frame fused to the 3′ end of the Flag-tag. For Flag-CTPsyn^{C399G} construction, we employed a mutagenesis technique to generate the mutated-CTPsyn fragments using the following specific primers: dCTPSC t1195g C399G F 5′-CCATTGCTTGGCATCGGCTTGGGTCTG CAAG -3′ and dCTPSC t1195g C399G R 5′-CTTGCAGACC CAAGCCGATGCCAAGCAATGG-3′. The DNA sequence of the product was confirmed before microinjection. For wild-type expression, *hs-Gal4::UAS-Flag-CTPsyn* transgenic flies were heat-shocked at 37° for 30 min and then incubated for 3 hr at 25°. Subsequently, ovaries were dissected and analyzed by immunostaining. For expression in *Cbl* mosaic egg chambers, *hsFlp/X;hs-Gal4/UAS-Flag-CTPsyn*; *CblFRT^{80B}/MycFRP^{80B}* were heat-shocked for 30 min/day. After 2 days of induction and incubation, the expression level of Flag-CTPsyn and occurrences of the S phase were examined by immunoblotting and by BrdU-incorporation assay, respectively.

Antibody generation

A total of 1–118 amino acids from *cg45070* (dCTPsyn in Flybase) was amplified by KOD-plus- DNA polymerase using the paired primers 5′-TAAGCAGAATTCATGAAATACATCCTGG TAACTG-3′ and 5′-ATTGCTCTCGAGAGTGATGTGTGGGACA ACTTG-3′ to clone the peptide into a *pET32a* vector, and 6× His fusion protein was purified by Ni-NTA beads (Qiagen). Antibodies were obtained by immunizing rabbit followed by affinity purification and then were used for Western blotting (1:1000).

Results

Ubiquitination is involved in the regulation of CTPsyn filamentous structure formation

An important insight into the developmental role of CTPsyn filaments can be derived from the identification of the biochemical switch that regulates its assembly. RNA silencing of CTPsyn led to the disassembly of CTPsyn filaments, suggesting that CTPsyn protein levels regulate the CTPsyn filament structure in a dose-dependent manner (Chen *et al.* 2011). To examine this hypothesis further, we treated *Drosophila* ovaries with MG132, a proteasome inhibitor that should block the degradation of CTPsyn, leading to an increase in

the number of CTPsyn structures. Surprisingly, a reduction in CTPsyn filament formation was found in both the germline cells and the follicle cells of egg chambers treated with MG132, compared to that in the DMSO control (Figure 1, A and B). The length of macro-cytoophidium in control egg chambers was 24.8 ± 7 μm on average, and this length was reduced to 11.6 ± 3.9 μm in egg chambers treated with MG132 (Figure 1I). On average, almost every follicle cell contained one CTPsyn filament (0.83 ± 0.05/per cell, Figure 1J), and a reduction in the number of filaments was observed with MG132 treatment (0.24 ± 0.14/cell, Figure 1J). Despite this observation, not all egg chambers were affected (Supporting Information, Figure S1D). The phenotype, however, did occur in all stages of oogenesis. Moreover, the inhibitory effect of MG132 on CTPsyn filament formation occurred in a dose-dependent manner with a higher dose resulting in a stronger inhibitory response (Figure S1, D and E). A similar, but somewhat less severe phenotype was observed in egg chambers expressing exogenous Flag-CTPsyn induced by hs-Gal4 (Figure S1, A and B). Nevertheless, the CTPsyn protein levels were comparable before and after MG132 treatment (Figure S1C).

We reasoned that MG132 treatment could result in two consequences: namely, blockage of protein degradation and depletion of free ubiquitin (Melikova *et al.* 2006). Given that CTPsyn protein levels remained largely unaffected, we next investigated whether overexpression of ubiquitin could suppress the effect of MG132. Indeed, selective expression of exogenous ubiquitin in follicle cells driven by CY2-Gal4 significantly reduced, from 0.24 ± 0.14/cell to 0.9 ± 0.1/cell, the MG132 effect on CTPsyn filament numbers (Figure 1J), indicating that ubiquitination may play a positive role in the regulation of CTPsyn filaments. In this *in vitro*-cultured ovary assay, the gradual disassembly of CTPsyn filaments (a "nil" phenotype that completely lacked filament) was observed in ~20% of egg chambers at 2 hr and in ~40% of egg chambers at 4 hr in medium containing DMSO (Figure 1K and Figure S1D). To further confirm that ubiquitin modification may play a positive role in filament formation, we next examined the effect of a deubiquitinase-inhibitor, Pr619. Indeed, the CTPsyn filament structures were preserved with Pr619 pretreatment for 2 hr followed by MG132 treatment (Figure 1, E–H and K). Together, these results suggest that ubiquitination is required to maintain CTPsyn filaments.

Since Cbl is an E3 ubiquitin ligase in follicle cells (Pai *et al.* 2000), we next investigated the role of *Cbl* in ubiquitin-mediated regulation of CTPsyn filaments using a genetic interaction assay with the *Prosβ6[1]* mutant. We used the allele *Prosβ6[1]*, a temperature-sensitive proteasome subunit mutant (Holden and Suzuki 1973; Saville and Belote 1993), and a *Cbl* null mutant, *Cbl[F165]* (Pai *et al.* 2000). At a nonpermissive temperature (29°), this dominant-negative *Prosβ6[1]* allele by itself did not show any significant difference from wild type (Figure 1L). However, the combination of *Cbl[F165]* and *Prosβ6[1]* displayed a synergistic effect on the negative regulation of CTPsyn filament formation (Figure 1, M–P and L), whereas the *Cbl* heterozygous mutant did not show significant effects. On average, every follicle cell contains 0.9, 1.0, and 0.9 CTPsyn filaments in OreR, *Cbl[F165]*/+, and *Prosβ6[1]*/+ egg chambers, respectively, but the number of CTPsyn filaments was reduced to 0.5 filaments/cell in *Cbl[F165]/Prosβ6[1]* egg chambers at a nonpermissive temperature (29°) (Figure 1L). Collectively, these results suggest that ubiquitination and *Cbl* may regulate the formation of CTPsyn filament structures.

Since disruption of Cbl E3 ligase activity enhances EGFR signaling in follicle cells (Pai *et al.* 2000; Wang and Pai 2011), we further assessed whether Cbl regulates CTPsyn filament structures through EGFR signaling. The CTPsyn filament was not affected by the overexpression of constitutively activated EGFR (λ-top) (Figure 1, Q–T) nor by activated Ras (*Ras[V12]*) (Figure S1, F–F′′) in follicle cells. In summary, Cbl regulates the formation of filament structures composed of CTPsyn through its E3 ligase activity and appears to do so independently of EGFR signaling.

Cbl regulates CTPsyn filaments without affecting CTPsyn protein levels

To elucidate the role of Cbl in regulating the formation of CTPsyn filament structure, mosaic *Cbl* mutant clones were generated in the follicular epithelium. In wild-type egg chambers, at least one CTPsyn filament was detected in every follicle cell (Figure 2, A and B) of stages 9–10 egg chambers. In contrast, few CTPsyn filaments were seen in *Cbl* mutant follicle cells (Figure 2, A–A′′ and B). We quantified the effects on CTPsyn filament formation by classifying the structures in each cell as (1) normal, (2) reduced in CTPsyn filament length (Figure 2D, "reduced"), or (3) the complete absence of CTPsyn filaments (Figure 2E, "nil"). A reduced phenotype was seen in 57% of *Cbl* mutant follicle cells, while 18% lacked CTPsyn filaments at stage 9. The defects became more severe at stage 10, when 36% of *Cbl* mutant cells exhibited a "reduced" phenotype and 58% showed a nil phenotype (Figure 2F). Similar defects in CTPsyn filaments were also observed in follicle cell mutants with another null allele of *Cbl* (*Cbl[BB28]*) (Figure S2, A–A′) (Pai *et al.* 2006). However, CTPsyn filaments were maintained as normal in *Cbl*-mutant cells when these cells were still in the mitotic stages of egg chamber development (before stage 6) (Figure S2, B–B′). To determine if this effect was specific for follicle cells, we examined another cell type that undergoes endocycles and that shows visible CTPsyn filaments, *i.e.*, the salivary glands (Figure 2G). Strikingly, CTPsyn filaments were also absent in the salivary glands of the *Cbl* mutant (Figure 2, H–H′). In contrast, the structure of the macro-cytoophidia in germline cells (nurse cells and the oocyte) was not obviously affected by the loss of *Cbl* (Figure S2D). The effects of Cbl on CTPsyn filament were confirmed by rescue experiments in which we ectopically expressed one of the two Cbl isoforms, CblL or CblS, in *Cbl* mutant follicle cells. Because overexpression of CblL induces lethality during development (Pai *et al.* 2006), we used D-CblL-PR^{Drk}, a full-length CblL carrying a point

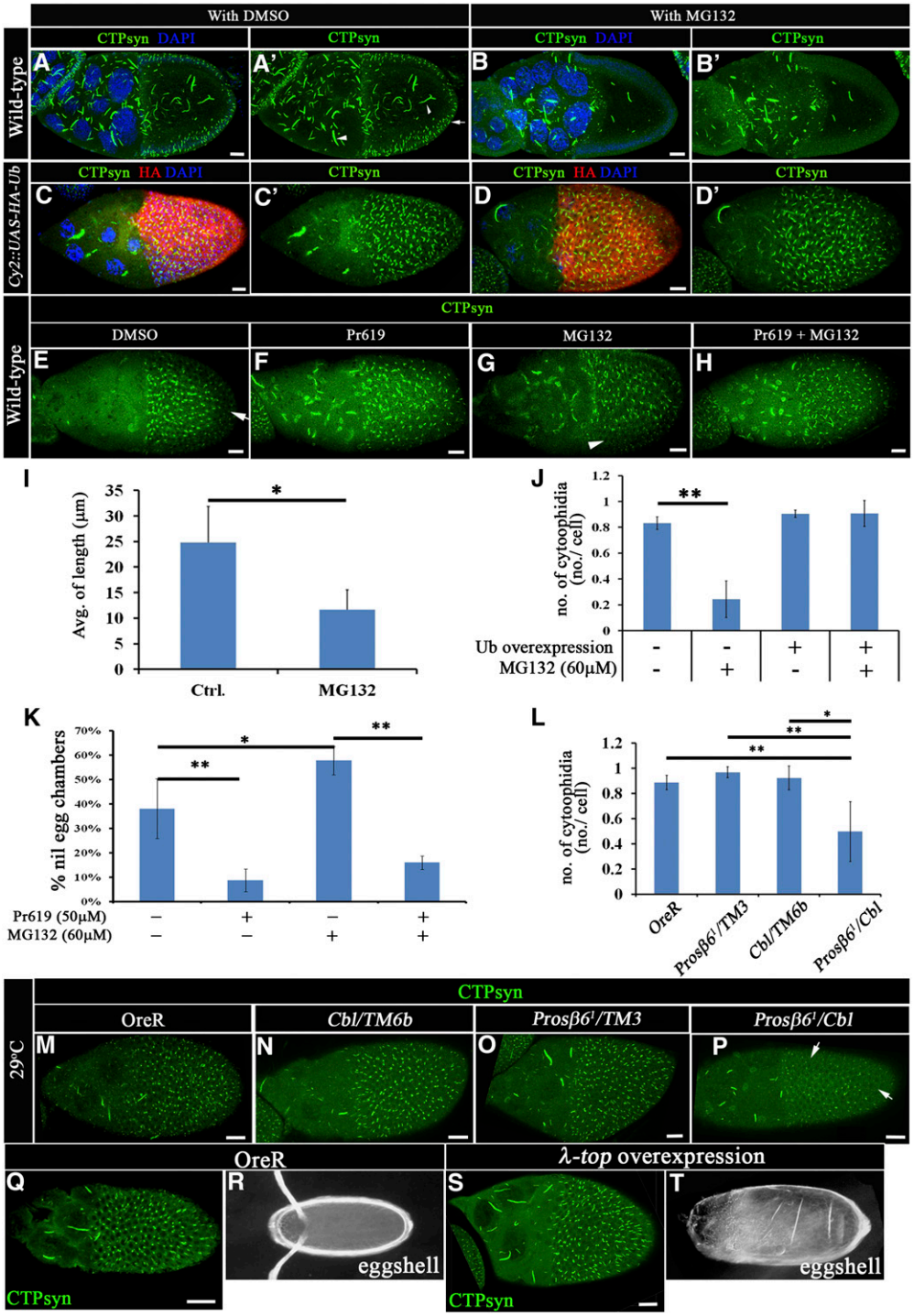

Figure 1 The proteasome degradation system is involved in the regulation of CTPsyn filaments. (A–B′) Merged-multiple confocal cross sections of middle-stage egg chambers stained with anti-CTPsyn antibody (green) and DAPI (blue). Macrocytoophidia are presented in germline cells (arrowhead), and CTPsyn filaments are shown in somatic cells (arrow). Wild-type egg chambers were treated with DMSO (as a control, A–A′) or 60 μM of the proteasome inhibitor MG132 (B–B′). The average length of macrocytoophidium was calculated after DMSO (control, 24.83 ± 7 μm) or 60 μM MG132 (11.67 ± 3.89 μm) treatment, and results are shown in I (n = 10 egg chambers, three biological replicates). (C–H, M–P, Q, and S) Merged multiple confocal surface sections of middle-stage egg chambers were stained with anti-CTPsyn antibody (green). (C–D′) Exogenous HA-ubiquitin-expressing (red) egg chambers were treated with DMSO (C–C′) or 60 μM MG132 (D–D′). The average number of CTPsyn filaments is shown in J (16, 51, 6, and 13 egg chambers for columns 1–4, respectively, with ∼140 follicle cells counted in each egg chamber). On average, the numbers of CTPsyn filaments/cell presented in DMSO- and MG132-treated wild-type egg chambers were 0.8 ± 0.5 and 0.24 ± 0.14, respectively. And the numbers of CTPsyn filaments/cell presented in DMSO- and MG132-treated HA-Ub-expressing egg chambers were 0.9 ± 0.03 and 0.9 ± 0.1, respectively. Wild-type egg chambers were treated with DMSO (E, affected region, arrow), MG132 (G, affected region, arrowhead), Pr619 (F), and MG132 plus Pr619 (H). The percentage of egg chambers showing nil phenotypes was calculated and is shown in K (191, 200, 180, and 187 egg chambers for columns 1–4, respectively, in three biological replicates). (M–P) Wild-type egg chambers (M), *Cbl*^{F165}/*TM6b* (N), *Pros*β*6*^{1}/*TM3* (O), and *Pros*β*6*^{1}/*Cbl*^{F165} (P, affected region, arrow) were incubated at a nonpermissive temperature (29°). The average number of CTPsyn filaments is shown in L (cells/egg chambers: 1255/5, 853/5, 1764/5, and 1021/5 for columns 1–4, respectively.). (Q) Wild-type and (S) λ-top-overexpressing egg chambers. (R and T) Eggs laid by wild-type females (R) or females carrying λ-top-overexpressing egg chambers (T). The results are shown as the mean ± SD; *$P < 0.05$ and **$P < 0.01$. Bar, 20 μm.

mutation in the Drk interaction motif (Wang and Pai 2011). D-CblL-PR^{Drk} and D-CblS each partially restored CTPsyn filaments, reducing the frequency of the nil phenotype of *Cbl* mutant cells at stage 10 from 79 to 34 and 42%, respectively (Figure S3, B–D). We next investigated whether the E3 ligase activity is required for Cbl-mediated CTPsyn filament maintenance by examining the ability of Cbl-D70Z, a Cbl isoform defective in E3 enzyme activity, to rescue the nil phenotype in *Cbl* mutant cells. The CTPsyn filament structure in follicle cells, however, could not be restored by D-Cbl-D70Z expression during stage 10 (Figure S3E), suggesting that E3 ligase activity is required for Cbl to maintain CTPsyn filaments.

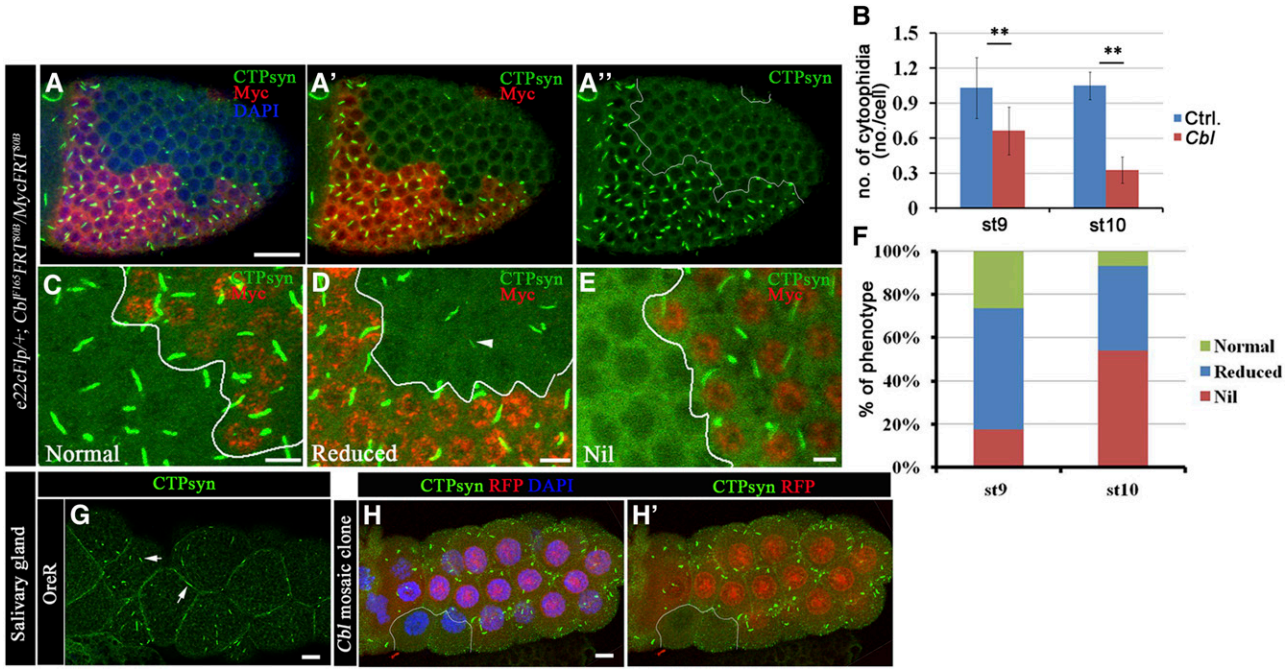

Figure 2 Cbl regulates the CTPsyn filamentous structure. (A–F) Merged confocal sections of stage 9–10 egg chambers stained with anti-CTPsyn (green) and anti-Myc (red) antibodies (A–A′′). Myc-positive signals marked wild-type and *Cbl* heterozygous cells, whereas *Cbl* homozygous mutant cells were marked by the absence of Myc staining. (B) Average numbers of CTPsyn filaments/cell were calculated from stage 9 and 10 egg chambers of the genotype *e22cFlp/+*; *Cbl* ^{F165}*FRT*^{80B}/*MycFRT*^{80B}. (C) Normal CTPsyn filament structures are shown in green and are represented by the green columns in F. The "reduced" phenotype (F, blue column) indicates a shortening (arrowhead in D) of CTPsyn filaments in *Cbl* mutant cells. The nil phenotype (red column) represents the lack of CTPsyn filaments (34 and 72 egg chambers at stages 9 and 10, respectively). (G) Larval salivary glands of OreR were stained with anti-CTPsyn antibody. CTPsyn filamentous structures are shown in green (arrow). (H–H′) Larval salivary glands containing a clone of *Cbl* mutant cells are marked by the absence of RFP (outlined in white) and stained with anti-CTPsyn (green) antibody. The results are shown as the mean ± SD; $^{**}P < 0.01$. Bar, 20 μm.

Taken together, these results demonstrate that *Cbl* regulates the formation of CTPsyn filament structures through its E3 ligase activity.

To investigate whether disruption of CTPsyn filament structures in *Cbl* mutant cells is caused by protein degradation, we first treated egg chambers with the CTPsyn inhibitor DON, an analog of glutamine, which blocks glutamine hydrolysis and promotes the formation of CTPsyn filaments in wild-type flies (Chen *et al.* 2011). Strikingly, the CTPsyn filament structure was restored by DON treatment in *Cbl* mutant follicle cells (Figure 3, B–B′) and salivary glands (Figure 3E). In contrast, the CTPsyn filament structures could not be rescued in CTPsyn-depleted follicle cells that were produced by RNA interference (RNAi) knockdown (Figure S4, D and E). To directly test whether loss of Cbl affected the levels of CTPsyn, we examined *Cbl* mutant salivary glands, which, as we demonstrated above, lack normal CTPsyn filaments. Immunoblotting revealed that the protein levels of CTPsyn were not reduced in the absence of Cbl (Figure 3F). This was consistent with results from a previous study and suggests that DON may induce structural alteration in CTPsyn, leading to CTPsyn polymer formation (Barry *et al.* 2014). DON treatment did not show effects on CTPsyn filament in follicle cells expressing CTPsyn RNAi (Figure S4) and did not elevate CTPsyn protein levels in *Cbl* mutant salivary glands or mosaic egg chambers (Figure 3G). These results suggest that *Cbl* contributes to stabilization of the CTPsyn filament structure rather than maintenance of CTPsyn protein levels.

Cbl is involved in endoreplication

Nucleotide pools are important for DNA replication. In follicle cells, the mass production of eggshell proteins, including vitelline membrane and chorion proteins, are promoted by amplifying the DNA templates for mRNA synthesis via a series of endocycles, followed by gene amplification. This requires cells to ramp up DNA synthesis in a process that involves altering the cell cycle and DNA replication program (Calvi *et al.* 1998; Tower 2004; Lee *et al.* 2009). Since Cbl regulates the CTPsyn-composed filamentous structures, which may influence the balance of the nucleotide pool, we next examined whether Cbl plays a role in endocycles, using a BrdU incorporation assay in stages 9–10B of egg chambers. Different degrees of endocycle defect were found in *Cbl* mutant follicle cells: 30 and 13% of wild-type (Myc-positive) cells were BrdU-positive during stages 9 and 10A, respectively, compared to 13% (Figure 4, A–A′′ and D) and 6% (Figure 4, B–B′′ and D) in *Cbl* mutant cells, respectively. This defect was not observed in stage-10B egg chambers (Figure S5, A–A′′) in which gene amplification took over endocycles in follicle cells.

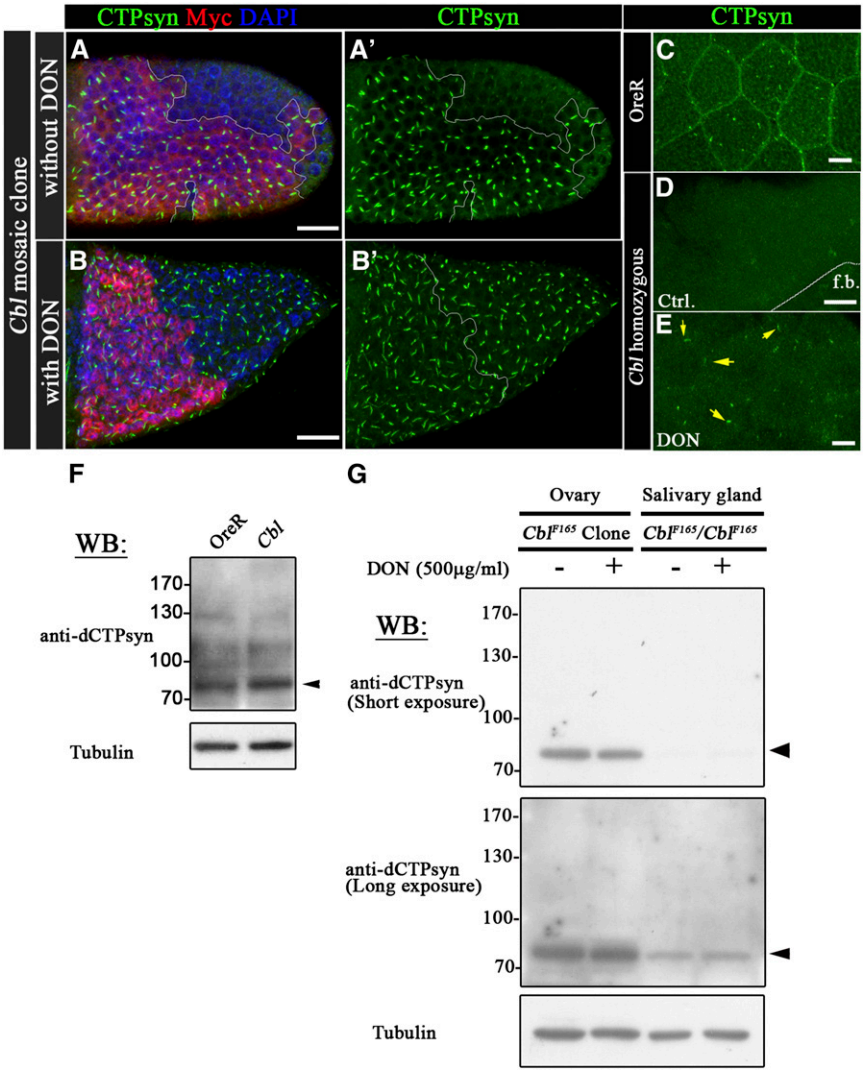

Figure 3 Cbl maintains CTPsyn filamentous structures without effects on CTPsyn protein levels. (A–B′) The labeling of cells is the same as described in Figure 2; *i.e.*, homozygous mutant cells are indicated by the absence of red Myc staining. (B–B′) CTPsyn filaments were restored partially in *Cbl* mutant cells through a 500-μg/ml DON treatment. (C–E) CTPsyn filaments were labeled with anti-CTPsyn antibody (green) in OreR and *Cbl* homozygous salivary glands with or without DON treatment. The CTPsyn filamentous structures were observed in *Cbl* homozygous salivary glands with DON treatment (arrow in E). (F–G) CTPsyn expression levels were analyzed by Western blots with anti-dCTPsyn antibody. Tubulin served as the loading control. Cell lysates were extracted from OreR, *Cbl* homozygous salivary glands (F), or *Cbl*-mosaic ovaries and *Cbl* homozygous salivary glands with or without DON treatment (G). f.b. indicates fat bodies. Bar, 20 μm.

We further confirmed the effect of *Cbl* on endoreplication in another polyploid tissue, the salivary gland. While the *Cbl* homozygous larvae were of normal size, the size of the *Cbl* mutant salivary glands were decreased. Simultaneously, both the reduced DAPI nuclear signals and small nucleus size (Figure 4G′′, arrowheads) were found in *Cbl* mutants, which is consistent with previous reports that endoreplication was found to be positively correlated with cell size (Edgar and Orr-Weaver 2001). Therefore, we further measured the nuclear size and DAPI fluorescence intensity of cells in *Cbl*-mosaic egg chambers and salivary glands. On average, the nuclear sizes were not significantly different between cells in twin clones and *Cbl* mutant clones, either in egg chambers or salivary glands (Figure S6, A and C). While the DAPI nuclear signal of *Cbl* mutant follicle cells showed no difference (Figure S6B), the DAPI signal was reduced in *Cbl* mutant salivary gland cells (Figure S6D).

Significantly reduced BrdU signals were found in *Cbl* homozygote mutant salivary glands (Figure 4G), indicating interference with the S phase of the endocycle. The density of the BrdU signal could be classified into three categories: bright, medium, and dark (Figure 4F′). The number of nuclei with a bright BrdU signal decreased by 18% in *Cbl* mutant cells, whereas the number of nuclei with dark BrdU signal increased by 21% (Figure S6F). The defect in endocycle occurrence might result from the loss of the license for cell cycle entry or from a defect in upstream Notch signaling. To determine whether the endocycle defect in *Cbl* mutant cells resulted from a CycE/Cdk2 activation defect, the number of cells recognized by an MPM2 monoclonal antibody was examined in *Cbl* mutant follicle cell clones. This antibody stains a subnuclear sphere of endocycling follicle cells and shows a positive correlation with CycE/Cdk2 activity (Calvi *et al.* 1998; White *et al.* 2007, 2011). The number of MPM2-positive cells did not change significantly in *Cbl* mutant clones (Figure 4, C–C′′ and E). This phenomenon was also observed in the salivary glands of *Cbl* mutants (Figure S5C). Similarly, by examining positive and negative effectors downstream of Notch in follicle cells, we demonstrated that Notch signaling was not altered either (Figure S7). These results indicate that Cbl is

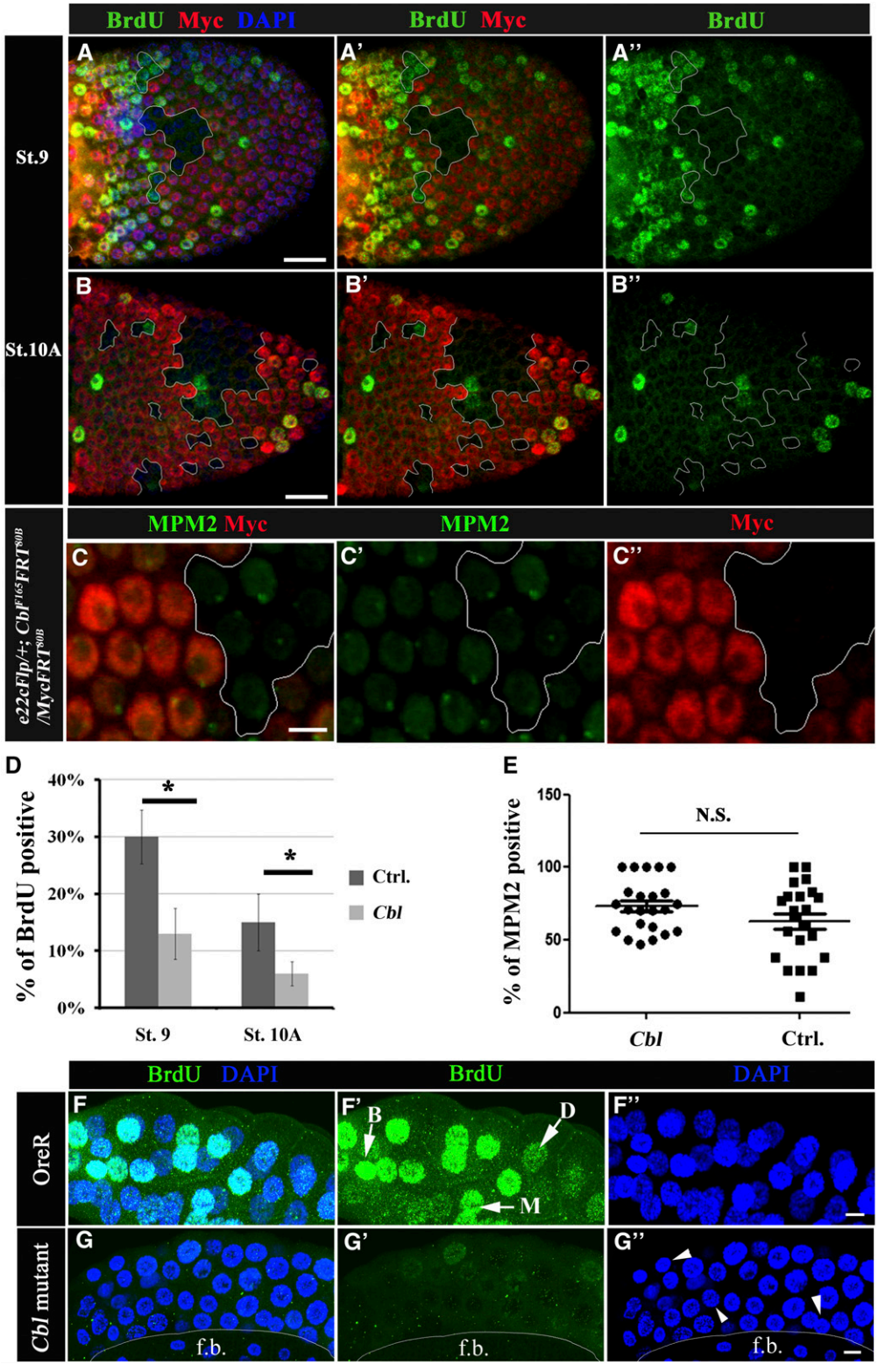

Figure 4 Cbl is involved in the endocycle. (A–C′′) Mosaic egg chambers containing *Cbl* mutant follicle cell clones. Cells are labeled as described in Figure 2. (A–B′′) BrdU incorporation is shown in the follicular epithelium containing mosaic clones for *Cbl* (Myc-negative cells, outlined in white) of stage 9 (A–A′′) and stage 10A (B–B′′) egg chambers. The BrdU signal is in green; nuclei were stained with DAPI (blue). (C–C′′) The MPM2 signal (in green) was detected in *Cbl* mutant cells and wild-type follicle cells in stage-9 egg chambers. (D) Percentages of BrdU-positive *vs.* Myc-negative cells (*Cbl*, light gray column) and Myc-positive twin clone cells with wild-type *Cbl* genes (Ctrl, dark gray column). Results are shown as the mean ± SEM; $*P < 0.05$. There were 16 and 18 egg chambers at stages 9 and 10, respectively. N = 3. (E) MPM2 positivity was assessed as described above; N.S. indicates not significant. (F–G′′) BrdU incorporation (shown in green) in wild-type (F–F′′) and in *Cbl* homozygous (G–G′′) salivary glands. In F′, BrdU signals were classified as bright (B), medium (M), or dark (D) (arrow). (F′′ and G′′) DNA was stained with DAPI (blue), and a reduction in nuclear size in *Cbl* mutant (arrowhead in G′′) was observed. f.b. indicates fat bodies. Bar, 20 μm.

involved in endocycle regulation and may act downstream of Notch signaling.

Depletion of CTPsyn disrupts endocycles in follicle cells

To further investigate whether CTPsyn activity is involved in the endocycle process, we examined DNA replication under CTPsyn depletion conditions. Dicer 2 (Dcr2) CTPsyn RNAi or GFP were driven by 55B-Gal4, which was expressed only in anterior follicle cells, allowing posterior follicle cells to serve as an internal control. Of the GFP-expressing control cells, 41% were BrdU-positive (Figure 5, A–A′ and C), while in CTPsyn-depleted cells the percentage of BrdU-positive cells

was decreased significantly to 2% (Figure 5, B–B′ and C). The number of MPM2-positive cells did not decrease under CTPsyn-depleted conditions (Figure S5E), suggesting that CTPsyn depletion could reduce DNA replication, but not entry into the S phase. The depletion of CTPsyn could lead to an imbalance in nucleotide pools, which could disrupt the endocycle event in *Drosophila* follicle cells. We further examined the relationship between Cbl and CTPsyn in endocycle regulation by investigating the endocycle in CTPsyn-depleted follicle cells in *Cbl* +/null mutants. The *Cbl* heterozygous and wild-type egg chambers showed similar percentages of BrdU-positive cells situated in the anterior follicular epithelium (Figure 5F). Silencing of CTPsyn without Dcr2 led to a reduction in BrdU-positive cells from 33 to 22% (Figure 5, D–D′ and F). The percentage of BrdU-positive cells decreased further to 16% (Figure 5, E–E′ and F) in a *Cbl* heterozygote background. In addition, the nuclear size of follicle cells was reduced from 31.2 to 24.0 and 19.9 μm in *CY2-Gal4/+;CTPsyn^{RNAi}/+* and *CY2-Gal4/+;CTPsyn^{RNAi}/Cbl^{F165}* stage-10A egg chambers, respectively (Figure S6E). Whereas *Cbl* heterozygous females generally produced normal eggs (Figure 5G), 21% of collapsed eggs were laid by females carrying a *Cbl* heterozygous mutation with CTPsyn depletion (Figure 5H). Therefore, Cbl interacts genetically with CTPsyn to regulate the endocycle. Taken together, Cbl may control the endocycle by maintaining the nucleotide pool balance in *Drosophila* follicle cells.

Cbl regulates endocycle by modulating CTPsyn activity

If the endoreplication defect in the *Cbl* mutant cell was due to an imbalance in nucleotides during the S phase, overexpression of CTPsyn might increase the activity of CTPsyn, rescuing the endoreplication defect. We found that exogenously expressed Flag-CTPsyn driven by hS-Gal4 could be incorporated into the CTPsyn filament structure in wild-type cells (Figure 6A), but that a CTPsyn filament structure was not seen in *Cbl* mutant cells despite overexpression of CTPsyn (Figure 6C). Nevertheless, the BrdU assay showed that overexpression of Flag-CTPsyn restored DNA replication from 16 to 25% in *Cbl* mutant cells (Figure 6, E–F′′ and Figure S8F). These results suggest that in *Cbl* mutant cells CTPsyn activity might not be adequate and that overexpression of CTPsyn could rescue this defect. If true, the catalytically defective mutant should not overcome the defect in *Cbl* mutant. Therefore, we generated a UAS-Flag-CTPsyn^{C399G} mutant, a mutation homologous to the C404G Ura7p mutant in yeast, which cannot bind its glutamine substrate (Noree *et al.* 2014). In agreement with our prediction, we found that this mutant could not restore the replication defect in *Cbl* mutant. Interestingly, this mutant also played a dominant-negative role in wild-type follicle cells (Figure 6G and Figure S8G), and in wild-type follicle cells, this Flag-CTPsyn^{C399G} mutant protein could be incorporated into a filament structure that contains endogenous wild-type CTPsyn (Figure 6B). Moreover, the Flag- CTPsyn^{C399G} mutant still formed filament structures in *Cbl* mutant follicle cells at similar expression levels to the wild-type CTPsyn (Figure 6D and Figure S8A), suggesting that the Flag-CTPsyn^{C399G} mutant protein escapes Cbl-mediated regulation in the process of CTPsyn filament formation. Glutamine depletion has been shown to induce the formation of CTPsyn polymers in a cell culture system (Calise *et al.* 2014). A similar effect on CTPsyn filaments was found in *Drosophila* S2 cells (Figure S8B′). To our surprise, this mutant could form filament structure in S2 cells in complete Schneider's *Drosophila* medium (Figure S8B′), indicating that the polymerization process of this mutant may differ from that of wild-type CTPsyn. In sum, Cbl influences endocycles by affecting the nucleotide pool balance and is required for wild-type CTPsyn to form filaments.

Next, we investigated whether Cbl-mediated regulation of filament formation is through direct ubiquitination of CTPsyn. The lysates of *Drosophila* S2 cells expressing HA-ubiquitin and Flag-CTPsyn were subjected to immunoprecipitation using anti-Flag antibody, and HA signals were detected in the immunoprecipitation products (Figure S8C). Furthermore, lysates of ovarian and salivary gland cells expressing HA-ubiquitin and Flag-CTPsyn were analyzed under similar conditions. However, no ubiquitination signal on CTPsyn was detected in either ovaries or salivary glands (Figure S8, D and E). Collectively, these results suggest that Cbl-mediated regulation of CTPsyn filament formation in follicle cells or salivary glands is not through direct ubiquitination of the CTPsyn protein itself.

Discussion

In this study, we revealed ubiquitin modification as a regulatory mechanism for the assembly of CTPsyn filaments throughout all stages of oogenesis (Figure 1 and Figure S1). Moreover, we identified Cbl as a specific E3 ubiquitin ligase that maintains these structures during endocycles (Figure 2) and showed that *Cbl* mutation resulted in a endoreplication-associated defect in the endocycle S phase (Figure 4). We also demonstrated that CTPsyn activity is essential for endoreplication (Figure 5) and that overexpression of wild-type CTPsyn, but not the catalytically defective mutant, is capable of rescuing the endocycle defect in *Cbl* mutant cells (Figure 6, E–G, and Figure S8). These results suggest that the activity of CTPsyn is insufficient to provide nucleotides for rapid endoreplication in *Cbl* mutant cells. Disruption of the CTPsyn filamentous structure in the absence of Cbl (Figure 2) may account for the defects in endocycles.

The ubiquitin modification of proteins by polyubiquitination or multi-monoubiquitination serves as a posttranslational regulatory mechanism to control protein stability or protein–protein interactions, respectively (Sadowski *et al.* 2012). In the salivary glands of *Cbl* null larvae, the CTPsyn protein level was not diminished (Figure 3F), suggesting that Cbl and CTPsyn filament structures are not required for stabilization of CTPsyn. However, the fact that D-Cbl-D70Z could not restore CTPsyn filament structures in *Cbl* mutant cells indicates that the E3 ligase activity of Cbl is required for the

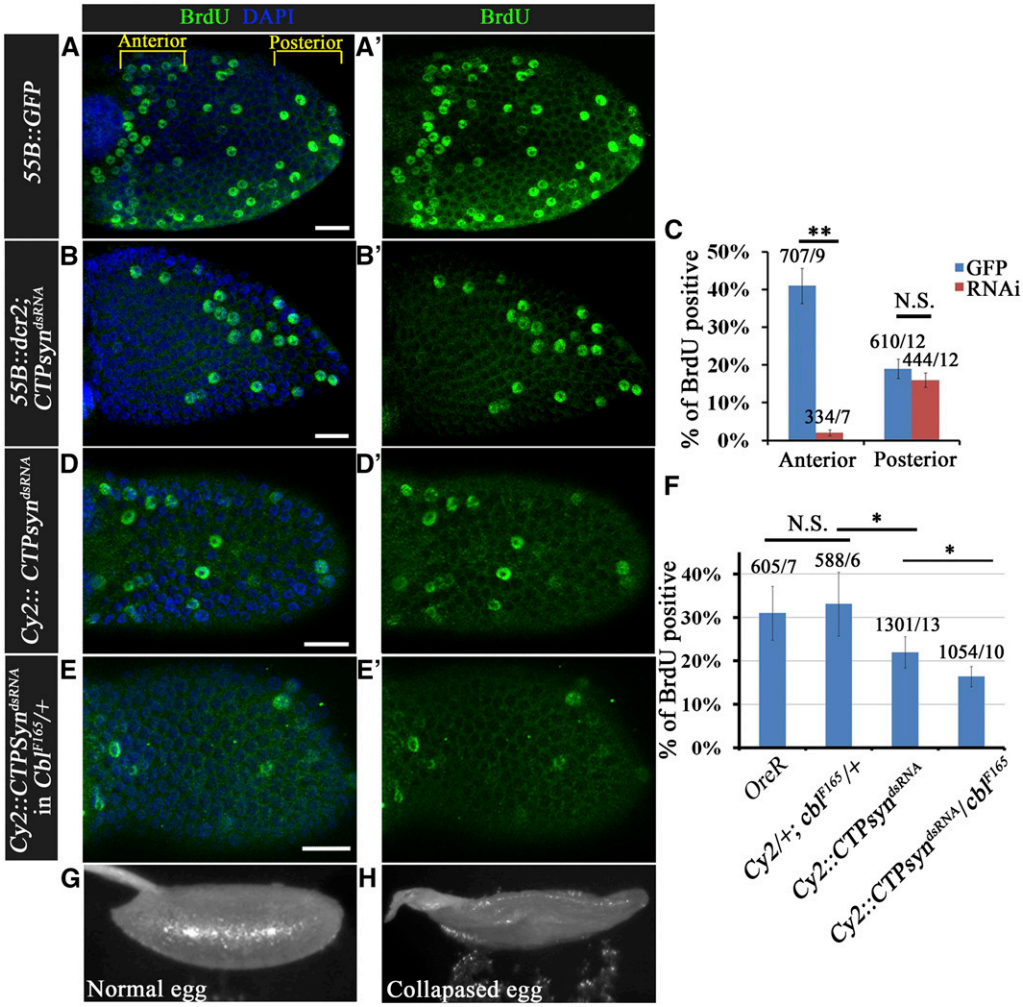

Figure 5 Cbl genetically interacts with CTPsyn. (A–B′) BrdU incorporation (green) was seen in stage-9 egg chambers expressing GFP (A–A′) or CTPsyn^{dsRNA} (B–B′) in their anterior follicle cells. (C) Quantification of BrdU-positive cells in the anterior and posterior regions of GFP-expressing (blue bars) or CTPsyn^{dsRNA}-expressing (red bars) egg chambers. (D–E′) BrdU incorporation was seen in follicle cells with CTP depletion in wild-type (D and D′) and *Cbl* heterozygous (E and E′) backgrounds. (F) Statistics for the percentage of BrdU-positive cells in the first five rows of anterior follicle cells/egg chamber with and without CTPsyn^{dsRNA} expression in wild-type and *Cbl* heterozygotes. (G) Wild-type eggshells and (H) collapsed eggshells laid by females with CTPsyn depletion in a *Cbl* heterozygous background. DNA was stained with DAPI (blue). Results are shown as the mean ± SEM; $*P < 0.05$ and $**P < 0.01$; N.S. indicates not significant. The numbers in C and F indicate the numbers of cells/egg chamber. Bar, 20 μm.

maintenance of the CTPsyn filament structure. In addition, we found that reversible ubiquitination regulates the dynamic assembly of both macro-and micro-cytoophidia in egg chambers. These results suggest that ubiquitination may provide a signal for polymerization of CTPsyn. While the activities of several enzymes have been reported to be controlled by ubiquitination-mediated protein degradation (Mattiroli and Sixma 2014) and by enzymatic inactivation through conformational changes (Sagar *et al.* 2007), the CTPsyn filament represents the first case in which an enzyme polymeric structure is regulated by ubiquitination.

Ubiquitin modification has been found in human CTPS1 using a proteomic approach (Udeshi *et al.* 2013). Our data indicate that Cbl-related ubiquitination of the CTPsyn protein itself might not occur in *Drosophila* follicle cells or salivary glands, suggesting that Cbl might act on an unknown protein that coordinates the formation of CTPsyn filament structures in an ubiquitination-dependent manner (Figure S8, D and E). We initially detected a CTPsyn filament-like structure using an antibody that was raised to recognize human phosphorylated PKD peptide. This structure was also recognized by anti-CTPsyn antibodies. Furthermore, even though *Drosophila* PKD has been excluded from the CTPsyn complex, we believe that CTPsyn is a complex that includes many types of enzymes, such as inosine-5′-monophosphate dehydrogenase and other proteins. This notion is supported by the recent finding that DAck colocalizes with CTPsyn filaments in germline cells (Strochlic *et al.* 2014).

Even though *Cbl* regulates CTPsyn filament structures only in follicle cells and not in germline cells, our inhibitor treatment assays and other genetic approaches in ovaries and other tissues demonstrated that CTPsyn filaments in germline cells, follicle cells, and salivary glands are sensitive to ubiquitin modification, suggesting that ubiquitination may be a general mechanism for the regulation of CTPsyn filament structures. Therefore, one possible explanation for the different effects of Cbl is that different cells may control CTPsyn filaments by different types of E3-mediated ubiquitination. Furthermore, the role of Cbl in CTPsyn filament formation seems to be crucial only in polyploid cells (Figure 2), such as follicle cells during the late endocycle stages (*i.e.*, stages 9–10A) and the salivary glands. In contrast, in diploid cells, such as follicle cells at the mitotic stage, CTPsyn filaments are normally maintained in *Cbl* mutant cells (Figure S2, B–B′). One possibility is that the endocycle places additional regulations on CTPsyn filament formation in follicle

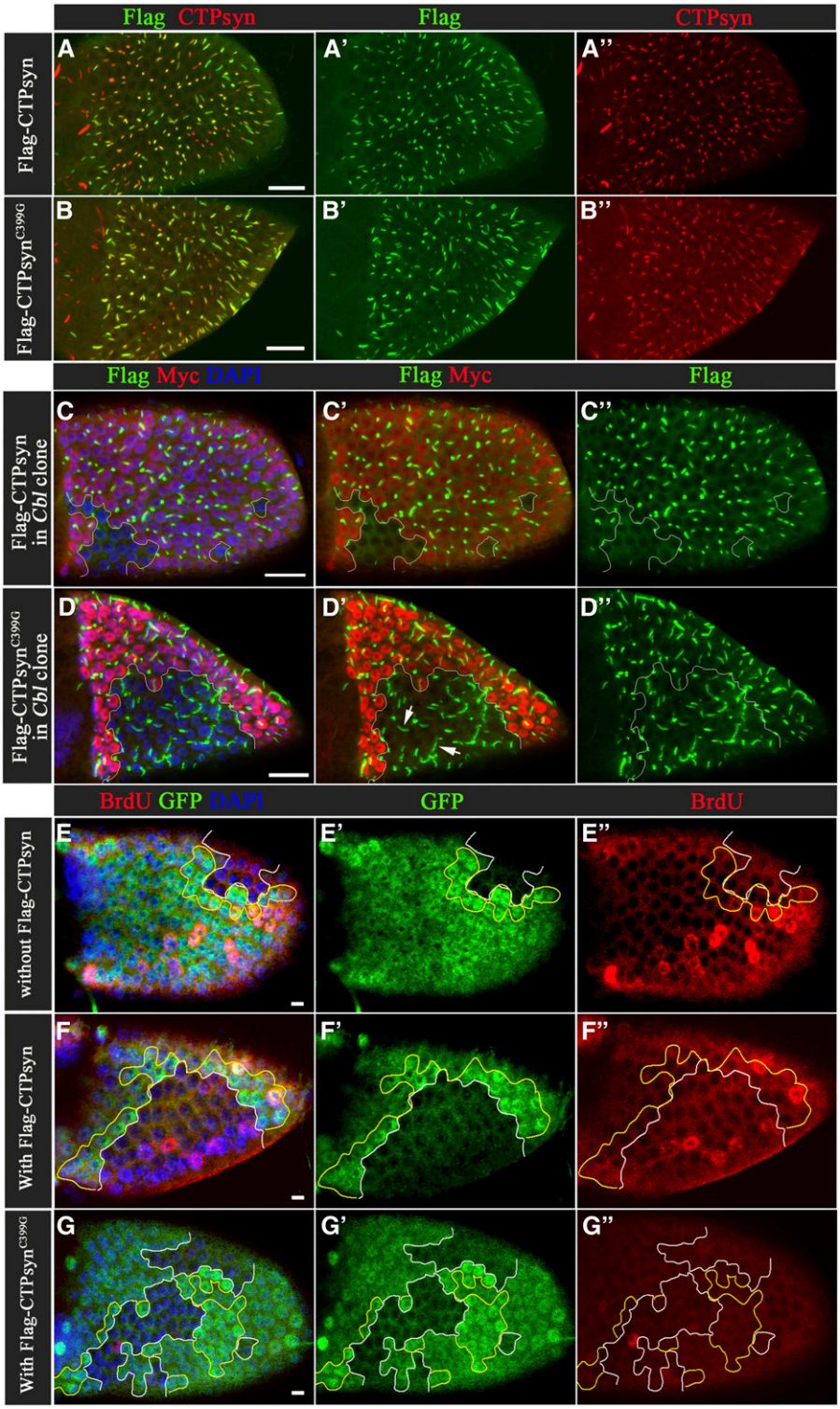

Figure 6 Cbl regulates endocycle through CTPsyn. (A–B'') Merged surface confocal sections of Flag-CTPsyn-overexpressing egg chambers were stained with anti-Flag (A' and B', green) and anti-CTPsyn (A'' and B'', red) antibodies. (C–D'') Multiple merged-surface confocal sections of Flag-CTPsyn-overexpressing egg chambers were stained with anti-Flag (green) antibody. The Flag-CTPsyn signal is shown in *Cbl*$^{+/+}$or *Cbl*$^{+/+}$cells (Myc-positive) and *Cbl*$^{-/-}$ follicular cells (Myc-negative). (E–G'') BrdU incorporation is shown in *Cbl* mosaic stage-9 egg chambers with or without Flag-CTPsyn transgene expression. *Cbl*$^{-/-}$ clone cells are marked by the absence of GFP (outlined in white), while *Cbl*$^{+/+}$ twin clone cells are marked by strong GFP-positive staining (outlined in yellow). BrdU signal is shown in red. DAPI-stained nuclei (blue). Bar: 20 μm (A–D) and 10 μm (E–G).

cells, such as increased dynamics of assembly/disassembly. We anticipated that, if Cbl-mediated ubiquitination is required for assembly, then the polymerization of CTPsyn filaments would be reduced in the absence of Cbl, while depolymerization would be unaffected, resulting in a net effect of filament shortening. Indeed, a range of effects on CTPsyn filament structures were seen in *Cbl* mutant cells, suggesting that further levels of regulation might affect the role of Cbl in the formation of CTPsyn filament structures. Further studies on the mechanisms of polymerization and depolymerization of CTPsyn filaments may provide greater insight into ubiquitination-mediated regulation.

It is conceivable that to adapt quickly for growth under various physiological conditions, cells must provide sufficient

materials to synthesize DNA, RNA, and lipids. Consistent with this interpretation, a special requirement for human CTP synthase1 (CTPS1) activity in DNA replication was revealed recently in receptor-mediated activation of T cells by anti-CD3 and anti-CD28 antibodies (Martin *et al.* 2014). The synthesis of phospholipids for membrane expansion is controlled by the levels of CTP, and the research group of Jeffrey R. Peterson at Fox Chase Cancer Center, Philadelphia, has demonstrated a role for CTPsyn in regulating the phospholipid composition of *Drosophila* germline cells (Chang and Carman 2008; Strochlic *et al.* 2014). Our results demonstrated that supplying the enzymatic activity of CTPsyn can restore endoreplication defects in *Cbl* mutant cells, indicating that Cbl may be involved in maintaining the nucleotide balance. During endocycles DNA replication reaches 16C within 24 hr in follicle cells and 1024C within 120 hr in the salivary glands. Loss of Cbl regulation resulted in a 50% reduction in DNA replication function (Figure 4D and Figure S6F). This defect could not be detected by measurement of nuclear size (Figure S6, A and C); however, it was reflected in the DAPI fluorescence signal in *Cbl* mutant salivary gland cells (Figure S6D). Given that in *Cbl* mutant cells CTPsyn filament structures are reduced, one possible explanation for these results is that CTPsyn filament structures are required to allow CTPsyn activity to meet the demand for nucleotide pools during endocycle. However, we still cannot exclude the possibility that Cbl regulates CTPsyn filament structures and CTPsyn activity independently.

Interestingly, CTPsyn filaments were observed under many specific physiological conditions. Nutrition depletion seems to be a common factor in the induction of this structure in yeast, brains of *Drosophila* larva, and mammalian cells (Aughey *et al.* 2014; Barry *et al.* 2014; Noree *et al.* 2010, 2014). In *Drosophila* S2 cells, we found that glutamine depletion induced filament formation, whereas normal Schneider's medium allowed very little filament formation. Interestingly, also, the glutamine-binding defect mutant C399G, an enzymatically inactive CTPsyn *in vivo*, seemed to mimic the wild-type CTPsyn in glutamine-depleted conditions so that filaments were formed in normal medium (Figure S8, B′ and B′′). Indeed, this mutant was not regulated by Cbl and formed filament structures in *Cbl* mutant cells. Given that this inactive mutant mingled with endogenous wild-type CTPsyn to form filaments, we hypothesize that CTPsyn filaments may be composed of different types of CTPsyn, including active, inactive, or a mixture of both forms.

CTP biosynthesis is one of several biosynthesis pathways implicated in liver malignancy and kidney carcinoma, and CTPsyn activity is increased in hepatomas (Williams *et al.* 1978). As the transition from tetraploidy to aneuploidy is considered to be an important step in cancer development (Davoli and de Lange 2011), the role of the proto-oncogene Cbl in the regulation of CTPsyn activity during endocycles implies a new mechanism through which Cbl promotes cancer formation. In this study, we defined a new role for the proto-oncogene Cbl in endocycles. We demonstrated that Cbl-mediated ubiquitination controls the assembly of CTPsyn filaments and may regulate the nucleotide supply for rapid endoreplication in *Drosophila*.

Acknowledgments

We thank Hai-Wei Pi, Fly Core Taiwan, the Bloomington Stock Center, and the Vienna Stock Center for providing the reagents and fly stocks; Trudi Schüpbach, Ji-Long Liu, Mark Peifer, Jörg Grosshans, Cheng-Ting Chien, Hai-Wei Pi, Bertrand Tan, Scott C. Schuyler, Tzu-Chien Van Wang, Chien-Kuo Lee, and Shu-Yuan Yang for commenting on the manuscript; and members of the Pai laboratory for their comments and helpful discussions. This work was supported by grants from the National Science Council of the Republic of China (NSC 101-2811-B-182-017 to P.-Y.W. and MOST103-2311-B-182-004-MY3 to L.-M.P.); the Chang Gung Memorial Hospital (CMRPD-2B0061-3 to L.-M.P.); and the Ministry of Education, Taiwan (EMRPD1E1421 to L.-M.P.).

Literature Cited

Anderson, P. M., 1983 CTP synthetase from Escherichia coli: an improved purification procedure and characterization of hysteretic and enzyme concentration effects on kinetic properties. Biochemistry 22: 3285–3292.

Aronow, B., and B. Ullman, 1987 In situ regulation of mammalian CTP synthetase by allosteric inhibition. J. Biol. Chem. 262: 5106–5112.

Aughey, G. N., S. J. Grice, Q. J. Shen, Y. Xu, C. C. Chang *et al.*, 2014 Nucleotide synthesis is regulated by cytoophidium formation during neurodevelopment and adaptive metabolism. Biol. Open 3: 1045–1056.

Azzam, G., and J. L. Liu, 2013 Only one isoform of Drosophila melanogaster CTP synthase forms the cytoophidium. PLoS Genet. 9: e1003256.

Barry, R. M., A. F. Bitbol, A. Lorestani, E. J. Charles, C. H. Habrian *et al.*, 2014 Large-scale filament formation inhibits the activity of CTP synthetase. eLife 3: e03638.

Buszczak, M., S. Paterno, D. Lighthouse, J. Bachman, J. Planck *et al.*, 2007 The carnegie protein trap library: a versatile tool for *Drosophila* developmental studies. Genetics 175: 1505–1531.

Calise, S. J., W. C. Carcamo, C. Krueger, J. D. Yin, D. L. Purich *et al.*, 2014 Glutamine deprivation initiates reversible assembly of mammalian rods and rings. Cell. Mol. Life Sci. 71: 2963–2973.

Calvi, B. R., and A. C. Spradling, 1999 Chorion gene amplification in Drosophila: a model for metazoan origins of DNA replication and S-phase control. Methods 18: 407–417.

Calvi, B. R., M. A. Lilly, and A. C. Spradling, 1998 Cell cycle control of chorion gene amplification. Genes Dev. 12: 734–744.

Carcamo, W. C., M. Satoh, H. Kasahara, N. Terada, T. Hamazaki *et al.*, 2011 Induction of cytoplasmic rods and rings structures by inhibition of the CTP and GTP synthetic pathway in mammalian cells. PLoS One 6: e29690.

Chakraborty, K. P., and R. B. Hurlbert, 1961 Role of glutamine in the biosynthesis of cytidine nucleotides in Escherichia coli. Biochim. Biophys. Acta 47: 607–609.

Chang, W. L., W. Liou, H. C. Pen, H. Y. Chou, Y. W. Chang *et al.*, 2008 The gradient of Gurken, a long-range morphogen, is directly regulated by Cbl-mediated endocytosis. Development 135: 1923–1933.

Chang, Y. F., and G. M. Carman, 2008 CTP synthetase and its role in phospholipid synthesis in the yeast Saccharomyces cerevisiae. Prog. Lipid Res. 47: 333–339.

Chen, K., J. Zhang, O. Y. Tastan, Z. A. Deussen, M. Y. Siswick *et al.*, 2011 Glutamine analogs promote cytoophidium assembly in human and Drosophila cells. J. Genet. Genomics 38: 391–402.

Davoli, T., and T. de Lange, 2011 The causes and consequences of polyploidy in normal development and cancer. Annu. Rev. Cell Dev. Biol. 27: 585–610.

Deng, W. M., C. Althauser, and H. Ruohola-Baker, 2001 Notch-Delta signaling induces a transition from mitotic cell cycle to endocycle in Drosophila follicle cells. Development 128: 4737–4746.

Edgar, B. A., and T. L. Orr-Weaver, 2001 Endoreplication cell cycles: more for less. Cell 105: 297–306.

Endrizzi, J. A., H. Kim, P. M. Anderson, and E. P. Baldwin, 2004 Crystal structure of Escherichia coli cytidine triphosphate synthetase, a nucleotide-regulated glutamine amidotransferase/ATP-dependent amidoligase fusion protein and homologue of anticancer and antiparasitic drug targets. Biochemistry 43: 6447–6463.

Epstein, A. M., C. R. Bauer, A. Ho, G. Bosco, and D. C. Zarnescu, 2009 Drosophila Fragile X protein controls cellular proliferation by regulating cbl levels in the ovary. Dev. Biol. 330: 83–92.

Gou, K. M., C. C. Chang, Q. J. Shen, L. Y. Sung, and J. L. Liu, 2014 CTP synthase forms cytoophidia in the cytoplasm and nucleus. Exp. Cell Res. 323: 242–253.

Holden, J. J., and D. T. Suzuki, 1973 Temperature-sensitive mutations in Drosophila melanogaster. XII. The genetic and developmental effects of dominant lethals on chromosome 3. Genetics 73: 445–458.

Ingerson-Mahar, M., A. Briegel, J. N. Werner, G. J. Jensen, and Z. Gitai, 2010 The metabolic enzyme CTP synthase forms cytoskeletal filaments. Nat. Cell Biol. 12: 739–746.

Klusza, S., and W. M. Deng, 2011 At the crossroads of differentiation and proliferation: precise control of cell-cycle changes by multiple signaling pathways in Drosophila follicle cells. BioEssays 33: 124–134.

Lee, H. O., J. M. Davidson, and R. J. Duronio, 2009 Endoreplication: polyploidy with purpose. Genes Dev. 23: 2461–2477.

Levitzki, A., and D. E. Koshland, Jr., 1971 Cytidine triphosphate synthetase. Covalent intermediates and mechanisms of action. Biochemistry 10: 3365–3371.

Levitzki, A., and D. E. Koshland, Jr., 1972 Role of an allosteric effector. Guanosine triphosphate activation in cytosine triphosphate synthetase. Biochemistry 11: 241–246.

Lieberman, I., 1956 Enzymatic amination of uridine triphosphate to cytidine triphosphate. J. Biol. Chem. 222: 765–775.

Lilly, M. A., and A. C. Spradling, 1996 The Drosophila endocycle is controlled by Cyclin E and lacks a checkpoint ensuring S-phase completion. Genes Dev. 10: 2514–2526.

Liu, J. L., 2010 Intracellular compartmentation of CTP synthase in Drosophila. J. Genet. Genomics 37: 281–296.

Long, C. W., and A. B. Pardee, 1967 Cytidine triphosphate synthetase of Escherichia coli B. I. Purification and kinetics. J. Biol. Chem. 242: 4715–4721.

Long, C. W., A. Levitzki, and D. E. Koshland, Jr., 1970 The subunit structure and subunit interactions of cytidine triphosphate synthetase. J. Biol. Chem. 245: 80–87.

Lopez-Schier, H., and D. St. Johnston, 2001 Delta signaling from the germ line controls the proliferation and differentiation of the somatic follicle cells during Drosophila oogenesis. Genes Dev. 15: 1393–1405.

Marmor, M. D., and Y. Yarden, 2004 Role of protein ubiquitylation in regulating endocytosis of receptor tyrosine kinases. Oncogene 23: 2057–2070.

Martin, E., N. Palmic, S. Sanquer, C. Lenoir, F. Hauck *et al.*, 2014 CTP synthase 1 deficiency in humans reveals its central role in lymphocyte proliferation. Nature 510: 288–292.

Mattiroli, F., and T. K. Sixma, 2014 Lysine-targeting specificity in ubiquitin and ubiquitin-like modification pathways. Nat. Struct. Mol. Biol. 21: 308–316.

Melikova, M. S., K. A. Kondratov, and E. S. Kornilova, 2006 Two different stages of epidermal growth factor (EGF) receptor endocytosis are sensitive to free ubiquitin depletion produced by proteasome inhibitor MG132. Cell Biol. Int. 30: 31–43.

Noree, C., B. K. Sato, R. M. Broyer, and J. E. Wilhelm, 2010 Identification of novel filament-forming proteins in Saccharomyces cerevisiae and Drosophila melanogaster. J. Cell Biol. 190: 541–551.

Noree, C., E. Monfort, A. K. Shiau, and J. E. Wilhelm, 2014 Common regulatory control of CTP synthase enzyme activity and filament formation. Mol. Biol. Cell 25: 2282–2290.

Pai, L. M., G. Barcelo, and T. Schupbach, 2000 D-cbl, a negative regulator of the Egfr pathway, is required for dorsoventral patterning in Drosophila oogenesis. Cell 103: 51–61.

Pai, L. M., P. Y. Wang, S. R. Chen, G. Barcelo, W. L. Chang *et al.*, 2006 Differential effects of Cbl isoforms on Egfr signaling in Drosophila. Mech. Dev. 123: 450–462.

Queenan, A. M., A. Ghabrial, and T. Schupbach, 1997 Ectopic activation of torpedo/Egfr, a Drosophila receptor tyrosine kinase, dorsalizes both the eggshell and the embryo. Development 124: 3871–3880.

Sadowski, M., R. Suryadinata, A. R. Tan, S. N. Roesley, and B. Sarcevic, 2012 Protein monoubiquitination and polyubiquitination generate structural diversity to control distinct biological processes. IUBMB Life 64: 136–142.

Sagar, G. D., B. Gereben, I. Callebaut, J. P. Mornon, A. Zeold *et al.*, 2007 Ubiquitination-induced conformational change within the deiodinase dimer is a switch regulating enzyme activity. Mol. Cell. Biol. 27: 4774–4783.

Saville, K. J., and J. M. Belote, 1993 Identification of an essential gene, l(3)73Ai, with a dominant temperature-sensitive lethal allele, encoding a Drosophila proteasome subunit. Proc. Natl. Acad. Sci. USA 90: 8842–8846.

Shcherbata, H. R., C. Althauser, S. D. Findley, and H. Ruohola-Baker, 2004 The mitotic-to-endocycle switch in Drosophila follicle cells is executed by Notch-dependent regulation of G1/S, G2/M and M/G1 cell-cycle transitions. Development 131: 3169–3181.

Strochlic, T. I., K. P. Stavrides, S. V. Thomas, E. Nicolas, A. M. O'Reilly *et al.*, 2014 Ack kinase regulates CTP synthase filaments during Drosophila oogenesis. EMBO Rep. 15: 1184–1191.

Tower, J., 2004 Developmental gene amplification and origin regulation. Annu. Rev. Genet. 38: 273–304.

Udeshi, N. D., T. Svinkina, P. Mertins, E. Kuhn, D. R. Mani *et al.*, 2013 Refined preparation and use of anti-diglycine remnant (K-epsilon-GG) antibody enables routine quantification of 10,000s of ubiquitination sites in single proteomics experiments. Mol. Cell. Proteomics 12: 825–831.

von der Saal, W., P. M. Anderson, and J. J. Villafranca, 1985 Mechanistic investigations of Escherichia coli cytidine-5′-triphosphate synthetase. Detection of an intermediate by positional isotope exchange experiments. J. Biol. Chem. 260: 14993–14997.

Wang, P. Y., and L. M. Pai, 2011 D-Cbl binding to Drk leads to dose-dependent down-regulation of EGFR signaling and increases receptor-ligand endocytosis. PLoS One 6: e17097.

Wang, Y., Z. Chen, and A. Bergmann, 2010 Regulation of EGFR and Notch signaling by distinct isoforms of D-cbl during Drosophila development. Dev. Biol. 342: 1–10.

White, A. E., M. E. Leslie, B. R. Calvi, W. F. Marzluff, and R. J. Duronio, 2007 Developmental and cell cycle regulation of the Drosophila histone locus body. Mol. Biol. Cell 18: 2491–2502.

White, A. E., B. D. Burch, X. C. Yang, P. Y. Gasdaska, Z. Dominski *et al.*, 2011 Drosophila histone locus bodies form by hierarchical recruitment of components. J. Cell Biol. 193: 677–694.

Williams, J. C., H. Kizaki, G. Weber, and H. P. Morris, 1978 Increased CTP synthetase activity in cancer cells. Nature 271: 71–73.

Communicating editor: R. J. Duronio

GENETICS

Supporting Information
www.genetics.org/lookup/suppl/doi:10.1534/genetics.115.180737/-/DC1

Regulation of CTP Synthase Filament Formation During DNA Endoreplication in *Drosophila*

Pei-Yu Wang, Wei-Cheng Lin, Yi-Cheng Tsai, Mei-Ling Cheng, Yu-Hung Lin, Shu-Heng Tseng, Archan Chakraborty, and Li-Mei Pai

DOI: 10.1534/genetics.115.180737

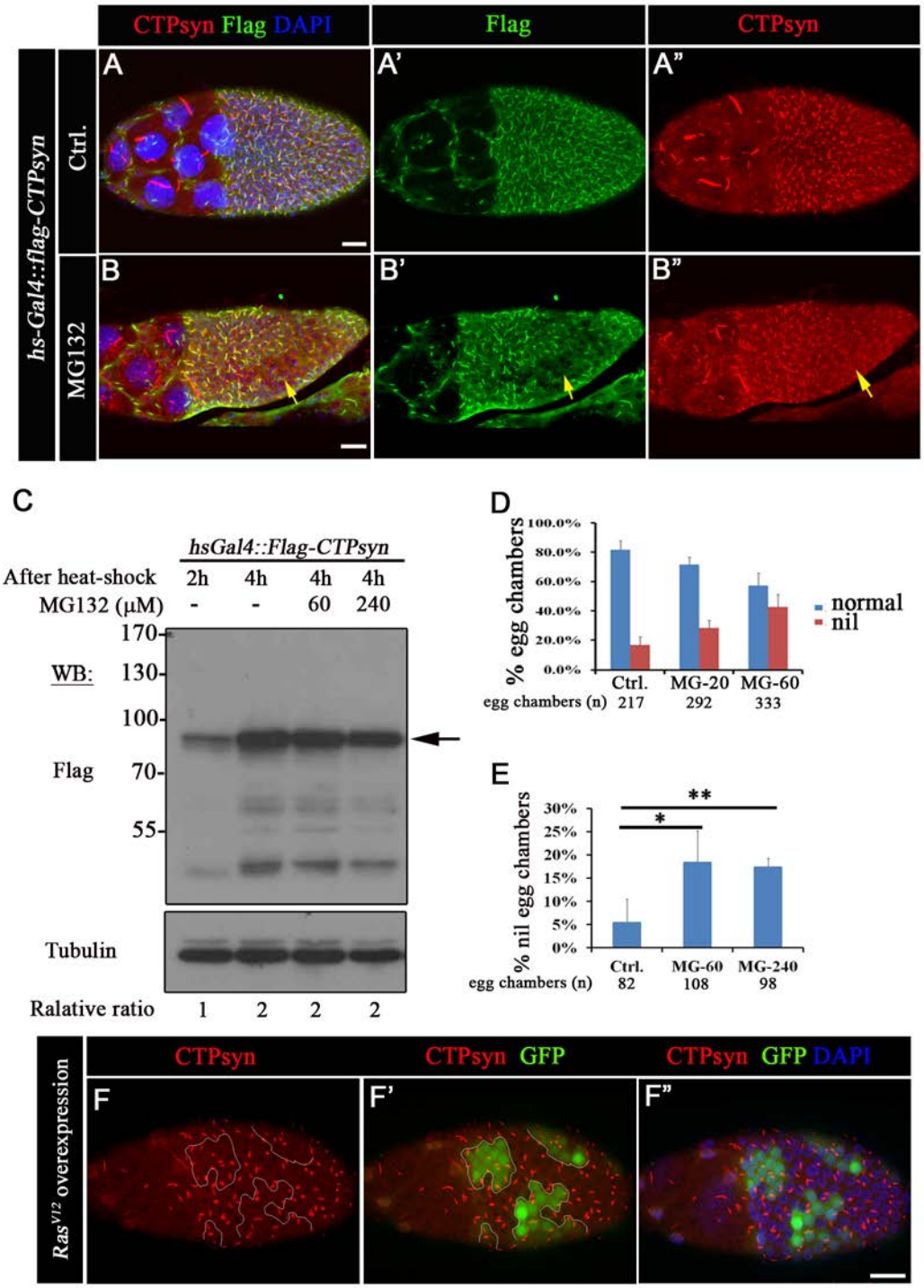

Figure S1. Inhibition of CTPsyn filament structures without altering CTPsyn protein levels. (A–B') Multiple merged-surface confocal sections of Flag-CTPsyn overexpressing egg chambers treated with DMSO (control, A–A") or 60 μM MG132

(B–B’) were stained with anti-Flag (green), anti-CTPsyn (red) and DAPI (blue, nuclei). (C) Western blot analysis of Flag-CTPsyn protein expression by anti-Flag antibody (arrow). Ovarian cell lysates were extracted from *hsGal4::Flag-CTPsyn* after heat shock for 2 h or 4 h, and treated with DMSO (-) or increasing doses of MG132. Tubulin was used as a loading control. Relative Flag-CTPsyn expression levels were analyzed with a densitometer and normalized to the level at 2 h. (D) Wild-type egg chambers were treated with DMSO, or 20 μM or 60 μM MG132. The percentage of nil phenotypes (red column) was calculated for DMSO (Ctrl. 16.6%), 20 μM MG132 (28.3%), and 60 μM MG132 (42.7%) treatments. (E) The percentages of nil phenotypes in stages 8–10A egg chambers with each indicated drug treatment were calculated. (F–F”) Multiple merged-surface confocal sections of stage 9 *RasV12* overexpressing (green) egg chambers stained with anti-CTPsyn (red) and DAPI (blue). The results are shown as the mean ± s.d.; $*p < 0.05$ and $**p < 0.01$. Scale bar: 20 μm.

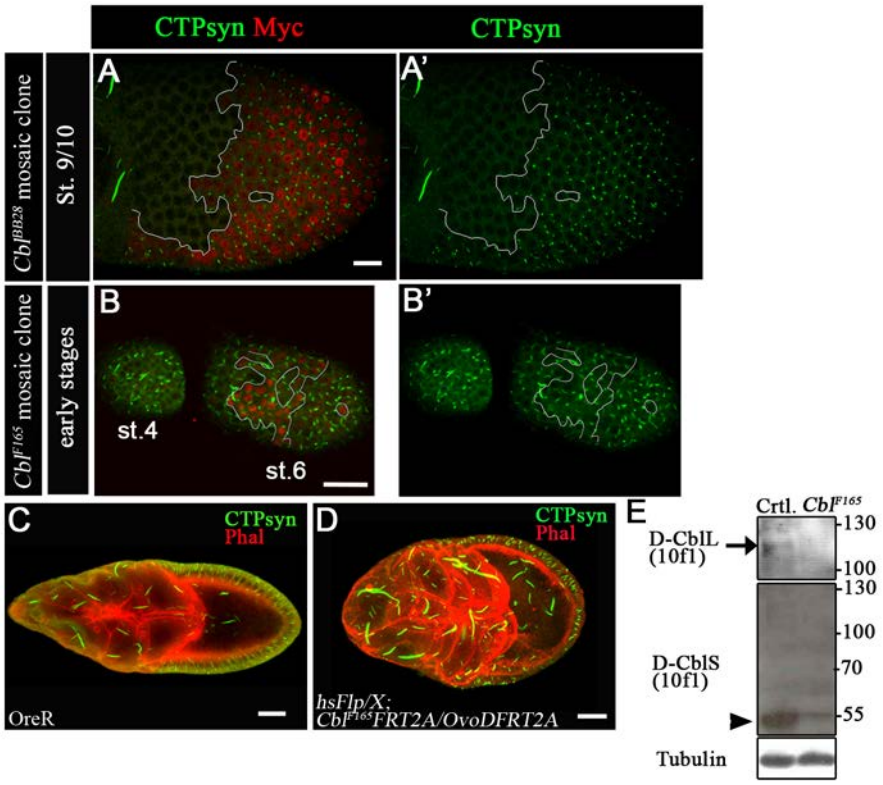

Figure S2. Cbl regulated CTPsyn filaments in follicle cells but not in the macro-cytoophidia of germline cells. (A–B') Multiple merged-confocal sections of stage 9 (A–A', *Cbl*^{BB28} allele), 4, or 6 (B–B', *Cbl*^{F165} allele) egg chambers were stained with anti-CTPsyn (green) and anti-Myc (red) antibodies. Myc signals represent *Cbl*$^{+/+}$ or *Cbl*$^{+/-}$ cells, and homozygous *Cbl* mutant cells lack any Myc signal. (C and D) Multiple merged cross sections of stage 9 egg chambers stained with anti-CTPsyn antibody (green) and phalloidin (red) in wild-type (C) and *Cbl* germline mutants (D). (E) The Cb1 protein expression levels analyzed with anti-D-Cbl antibodies (10F1) that recognize the D-Cbl long form (arrow) and D-Cbl short form (arrowhead). Tubulin was used as a loading control. Ovarian cell lysates were extracted from OreR (Ctrl) and *Cbl* germline mutants (genotype shown in D). Scale bar: 20 μm.

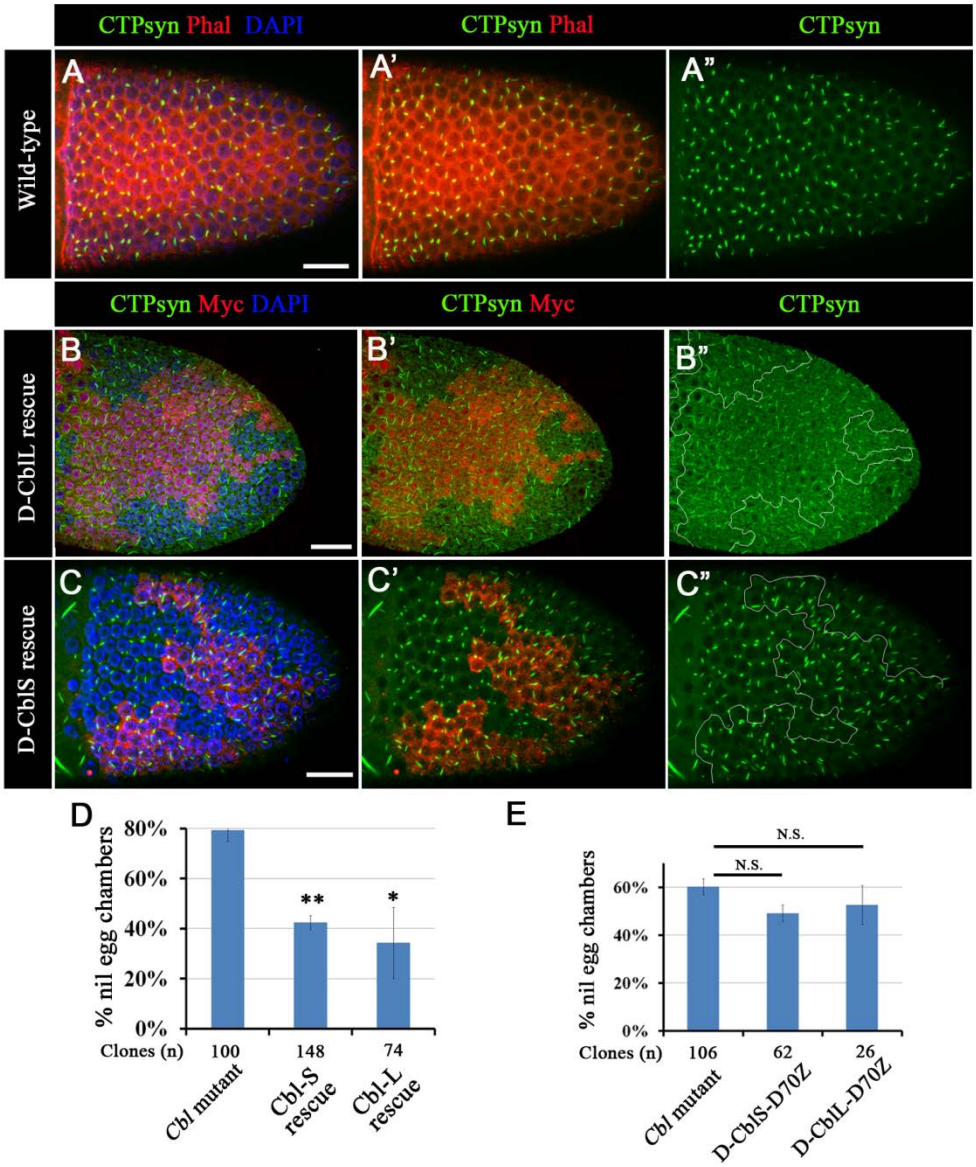

Figure S3. Both isoforms of Cbl partially rescued the defective phenotype of *Cbl* mutant cells. (A–A") Multiple surface confocal sections of the stage 9 wild-type egg chamber. CTPsyn filaments were revealed by anti-CTPsyn antibody (green). DNA was stained with DAPI (blue). Phalloidin is shown in red. (B–C") Mosaic egg

chambers containing *Cbl*^{F165} mutant follicle cell clones were labeled as described in Figure S2A. CTPsyn filaments were restored by constitutive expression of CblL-PR^{Drk} (B-B") and CblS (C-C") in *Cbl* mutant cells (Myc-negative). (D) The nil phenotype was calculated in *Cbl* mutant cells with or without CblL-PR^{Drk} or CblS expression in stage 10 egg chambers. (E) The nil phenotype was calculated in *Cbl* mutant cells with or without D-CblS-D70Z and D-CblL-D70Z rescued in stage 10. Results are shown as the mean ± s.e.m; **p* < 0.05 and ***p* < 0.01. N.S indicates not significant. Scale bar: 20 μm.

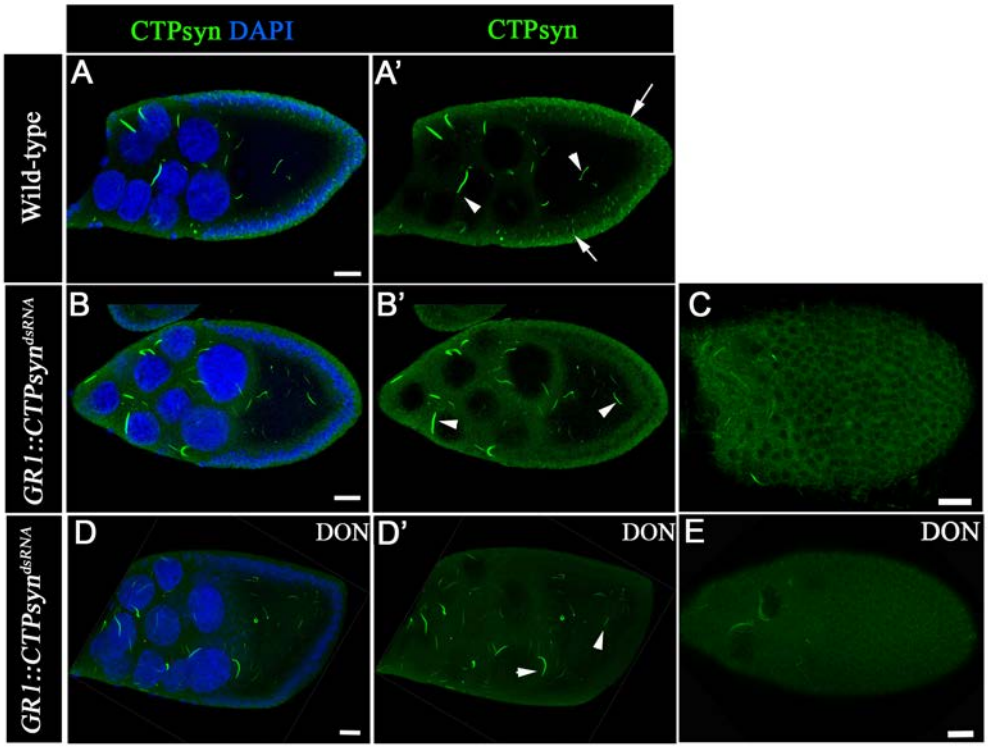

Figure S4. CTPsyn filament formation depends on CTPsyn protein levels in follicle cells. (A–E) Multiple confocal cross sections (A–A', B–B', D–D') and surface-sections (C, E) of stage 9 egg chambers were immunostained with anti-CTPsyn antibody (green) and DAPI (blue). (A–A') In the wild-type egg chamber, macro-cytoophidia were presented in the germline cells (arrowhead) and cytoophidia were presented in the main-body follicle cells (arrow). (B–C) Dcr2 and CTPsyn RNAi were co-overexpressed in the main-body follicle cells to reduce the level of CTPsyn. Macro-cytoophidia were not affected in the germline (arrowhead). (D–E) CTPsyn-depleted egg chambers were treated with 500 μg/ml DON. Scale bar: 20 μm.

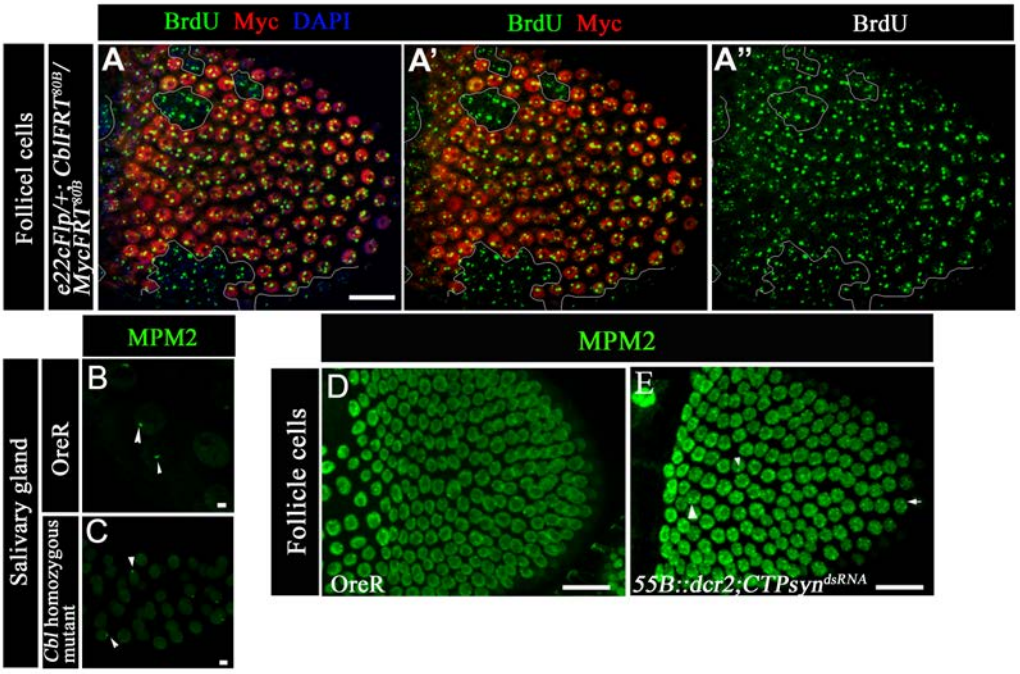

Figure S5. The effect of *Cbl* on the occurrence of S phase. (A-A") Mosaic egg chambers containing *Cbl* mutant follicle cell clones. Cells were labeled as described in Figure S2A. BrdU incorporation (green) is shown in the follicular epithelium containing mosaic clones for *Cbl* (Myc-negative cells, white lines) of stage 10B egg chambers. (B–C) MPM2 signals in wild-type (B) and *Cbl* homozygous (C) salivary glands. (D–E) The MPM2 signal (arrow) was detected in stage 9 egg chambers of wild-type posterior follicle cells (E, arrow) and in CTPsyn-depleted (E) anterior follicle cells expressing Dcr2 and CTPsyn^{RNAi}. The MPM2 signals did not differ significantly between anterior (arrowhead) and posterior follicle cells (arrow). Scale bar: 20 μm (A–A", D, E), 5 μm (B, C).

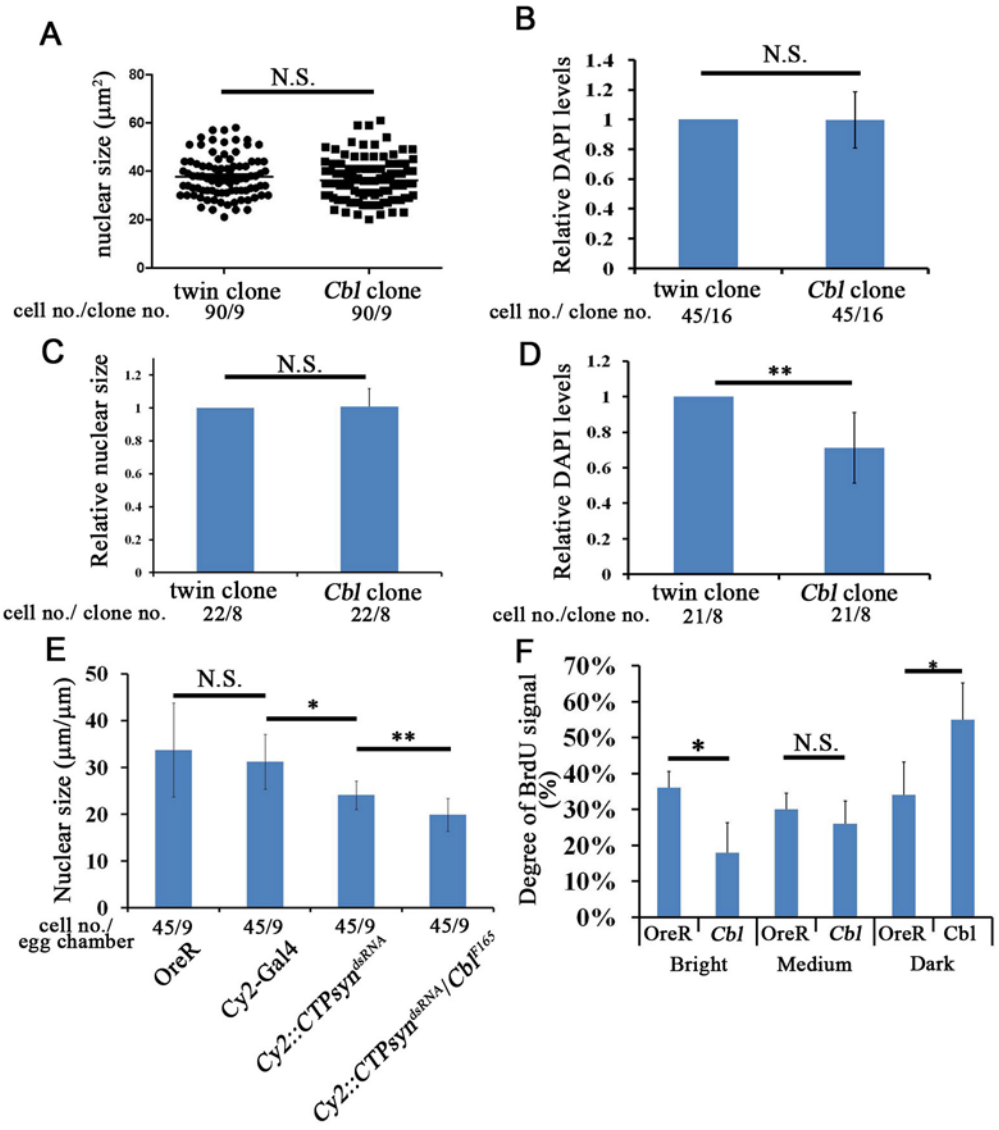

Figure S6. The effect of *Cbl* on nuclear size and intensity. (A and C) The nuclear size of twin clones and *Cbl* clones in egg chambers (A) or salivary glands (C) were measured. (B and D) The relative intensities of nuclear DAPI signal in twin wild-type and *Cbl* follicular clones of egg chambers (B) or salivary glands (D) were measured. (E) The nuclear sizes of follicle cells of egg chambers shown in Figure 5 were measured. (F) Percentages of BrdU classes in wild-type or *Cbl* homozygous salivary glands from three independent experiments. BrdU signals were classified as bright (B),

medium (M), or dark (D). Results are shown as the mean ± s.d.; *$p < 0.05$; ** $p < 0.01$; N.S.: not significant.

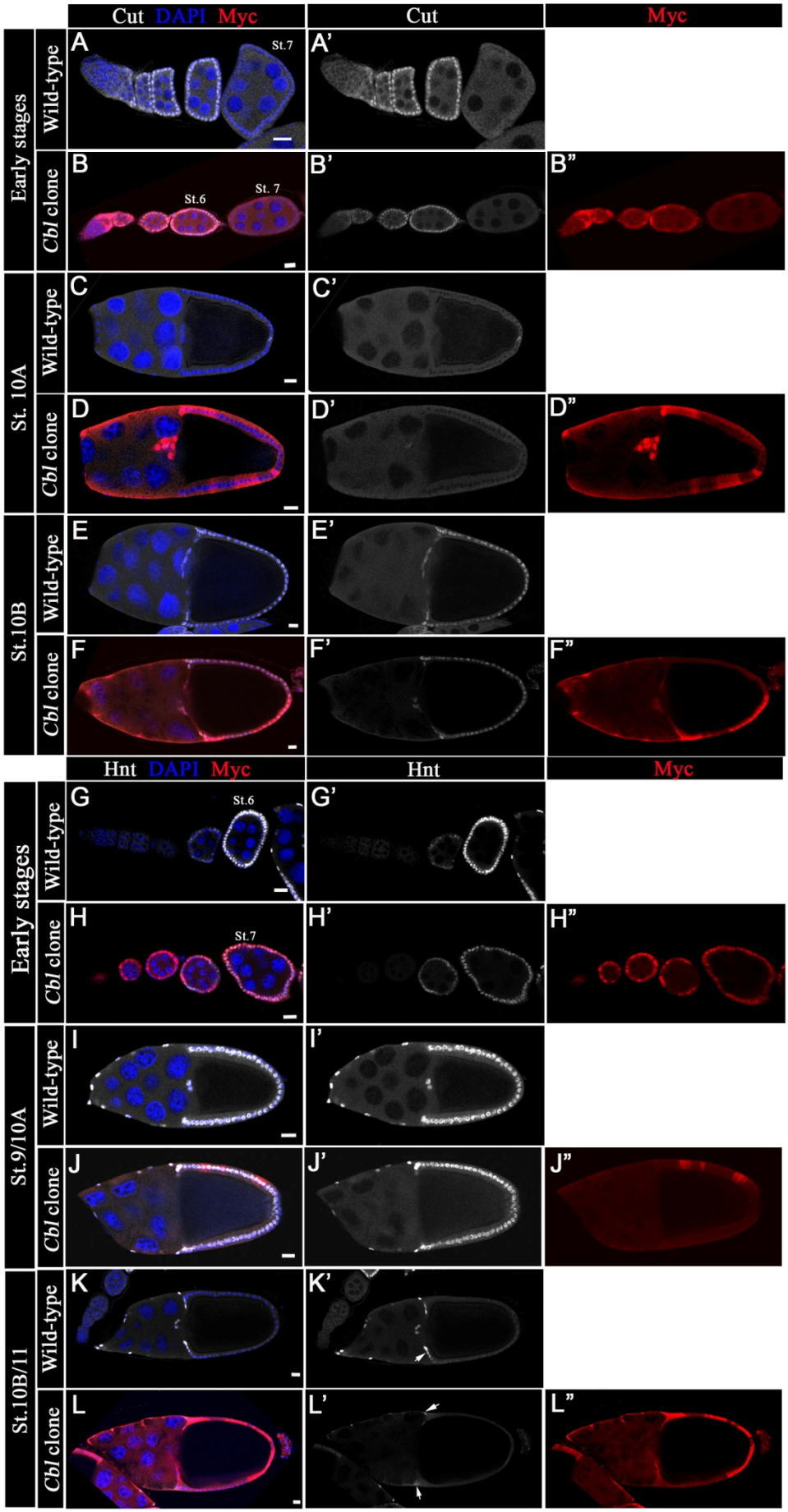
Cut DAPI Myc
Cut
Myc
Early stages
Wild-type
A
St.7
A'
Cbl clone
B
St.6
St. 7
B'
B"
St. 10A
Wild-type
C
C'
Cbl clone
D
D'
D"
St.10B
Wild-type
E
E'
Cbl clone
F
F'
F"
Hnt DAPI Myc
Hnt
Myc
Early stages
Wild-type
G
St.6
G'
Cbl clone
H
St.7
H'
H"
St.9/10A
Wild-type
I
I'
Cbl clone
J
J'
J"
St.10B/11
Wild-type
K
K'
Cbl clone
L
L'
L"

Figure S7. Notch signaling was not altered in *Cbl* mutant follicle cells.

(A–F”) Cut (white) and (G–L”) Hnt (white) staining in wild-type (A–A’, C–C’, E–E’, G–G’, I–I’, and K–K’) or *Cbl* mosaic egg chambers (B–B”, D–D”, F–F”, H–H”, J–J”, and L–L”). $Cbl^{+/+}$ or $Cbl^{+/-}$ cells were Myc-tagged. (A–B”) Expression of Cut in follicle cells of early-stage egg chambers (stages 1–6); (C–D”) at stage 9/10A; and (E–F”) at stages 10B/11. (G–J”) Expression of Hnt at stages 7–10A when Notch is activated and (K–L”) at stages 10B/11. Scale bar: 20 μm.

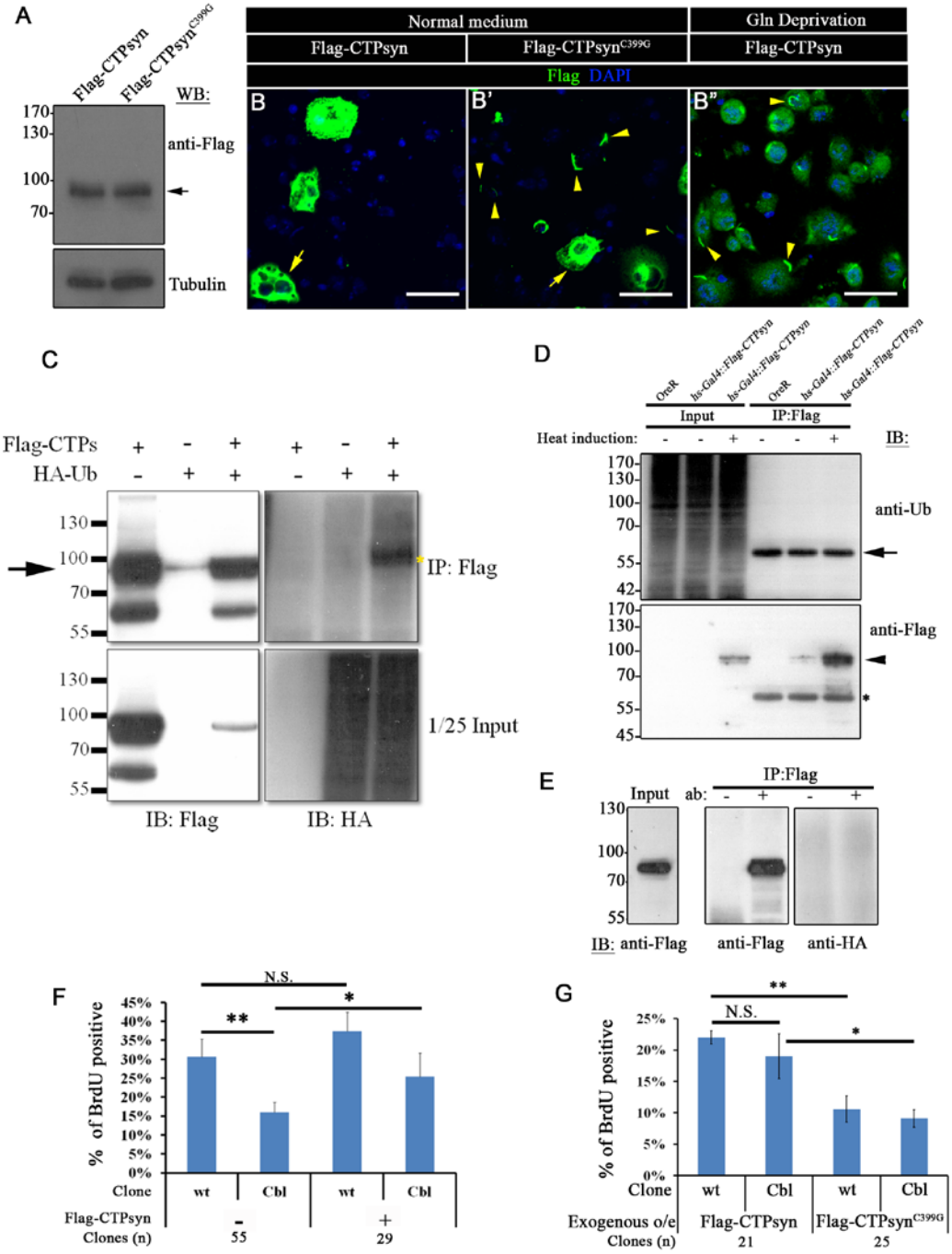

Figure S8. Cbl did not regulate CTPsyn filament structures through the ubiquitination of CTPsyn

(A) Exogenous Flag-CTPsyn expression levels were analyzed in ovarian lysates from *hs-Gal4::Flag-CTPsyn* and *hs-Gal4::UAS-Flag-CTPsyn*^{C399G} females using western

blot. Hs-Gal4 was first expressed at 37°C for 30 minutes and then switched to 25°C to express UAS-Flag- CTPsyn for an additional 3 h before lysing the cells for western blotting using anti-Flag antibody. Tubulin was used as a loading control. (B–B") Multiple merged-confocal sections of S2 cells incubated in complete (B–B') or glutamine-deficient (B") Schneider's medium were stained with anti-Flag (green) and DAPI (blue). The CTPsyn filament structures were observed in Flag-CTPsyn^{C399G}-transfected cells (arrowhead in B') in complete Schneider's medium, and in Flag-CTPsyn-transfected cells in glutamine-deficient medium (arrowhead in B"). Arrows indicate highly expressed cells. (C) Flag-CTPsyn was immunoprecipitated from transfected S2 cells that were co-transfected with HA-ubiquitin using anti-Flag antibody. The immunoprecipitated product was subjected to immunoblotting using anti-HA (right) or anti-Flag antibodies (left). The arrow indicates Flag-CTPsyn. The ubiquitinated protein signal is presented at the right (yellow star). (D and E) Flag-CTPsyn was immunoprecipitated from ovarian (D) or salivary gland (E) cell lysates by anti-Flag antibody. In this assay, ovaries expressed Flag-CTPsyn and salivary glands co-expresses HA-ubiquitin and Flag-CTPsyn. The products were subjected to immunoblotting using anti-Flag antibody (arrowhead in D), anti-ubiquitin (D), or anti-HA (E) antibody. The arrow in D indicates a non-specific band, and the heavy chains of antibodies are labeled by *. (F and G) The percentage of

BrdU-positive versus GFP-negative cells (white line in Figure 7), and GFP-positive cells (yellow line in Figure 7) was quantified per egg chamber. The egg chambers overexpressing Flag-CTPsyn or Flag-CTPsyn^{C399G} in main-body follicle cells. (n = 3 biological repeats). Scale bar: 20 μm. Results are shown as the mean ± s.d.; *$p < 0.05$; **$p < 0.01$, and N.S.: not significant.

File S1. Supplemental Experimental Procedures

Cell culture and transfection

S2 cells were transfected with UAS-Flag-dCTPsyn C form and UAS-HA-Ubiquitin using Effectine reagent (Qiagen), then cultured for 1 day in Schneider's *Drosophila* medium (Genaxxon) supplemented with 10% fetal bovine serum (FBS) and 1% antibiotic-antimycotic (Invitrogen), with or without L-glutamine.

Immunoprecipitation

S2 cells were transfected with UAS-Flag-dCTPsyn C form and UAS-HA-Ubiquitin using Effectine reagent (Qiagen), and then cultured in Schneider's *Drosophila* medium (Genaxxon) supplemented with 10% fetal bovine serum (FBS) and 1% antibiotic-antimycotic (Invitrogen). A total of 1 x 10^7 S2 cells were homogenized with lysis buffer. The ovarian lysates were extracted from ovaries of OreR and *hs-Gal4::CTPsyn* females, which were heat-shocked at 37°C for 30 min, and then incubated at 25°C for an additional 2 h before dissection. Salivary gland samples, 180 pairs, from 96h *CY2-Gal4::HA-Ub; Flag-CTPsyn* larvae were dissected in Schneider's *Drosophila* medium each time, and then stored at -80°C until reaching

1000 pairs (1 pair contains about 1 μg of proteins). Lysates were fractionated by centrifugation at 12000 *g* for 10 min at 4°C. The supernatants were incubated with anti-Flag antibody (1 μg/500 μg lysate) in lysis buffer (50 mM HEPES, 50 mM NaCl, 0.5% Doc, 1% Triton-100, 10 mM NEM, 5 mM EDTA, 1 mM EGTA, 10 mM NaF, 1 mM $NaVO_3$, and 1 × protease inhibitor) for 2 h at 4°C. Then, protein G sepharose beads were added to bring down the immunoprecipitates for 1 h at 4°C. Pellets were dissolved in 2 × sample buffer that was boiled for 10 min. The samples were resolved by SDS-PAGE, transferred to an NC membrane, and immunoblotted with anti-Flag (Sigma), anti-ubiquitin (P4D1, Santa Cruz) and anti-HA (Roche) antibodies.

Quantification of nuclear size and DAPI intensity

The quantification results of follicle cell/salivary gland nuclear sizes and the DAPI intensity of *Cbl* clone are shown in Figures S6A-D. In figure S6A, 90 pairs of cells of twin clone and of *Cbl* follicular mutant clone were analyzed. The stage 10A egg chamber confocal images came from 4 independent experiments. For DAPI intensity in follicle cells, 90 nuclei of sixteen *Cbl* clones from 7 independent experiments were analyzed. The relative intensity of DAPI signal was measured through dividing the signal of *Cbl* mutant cells by that of adjacent wild type cells. The intensity was determined by total intensity in a defined area divided by pixels inside the area. Since

the nucleus size of salivary gland was heterogenous along the proximal and distal axis, the relative nuclear size was measured through dividing the size of *Cbl* mutant cell nuclei by that of adjacent wild type cell nuclei. There are 22 pairs of cells in 8 clones from 3 independent experiments were analyzed. Twenty-one nuclei of 8 salivary glands from 4 independent experiments were analyzed on DAPI intensity. For nuclear sizes in figure 5, the average nuclear size of 45 cells from each genotype (random 5 cells in each egg chamber were selected from 3 independent experiments) were analyzed. The images were quantified using ZEISS LSM Image Browser software.